HHS Public Access

Author manuscript

Dev Cell. Author manuscript; available in PMC 2021 December 21.

Published in final edited form as:

Dev Cell. 2020 December 21; 55(6): 737–753.e7. doi:10.1016/j.devcel.2020.10.023.

N^6-Adenosine methylation of *Socs1* mRNA is required to sustain the negative feedback control of macrophage activation

Jie Du[1,2], **Wang Liao**[1,3], **Weicheng Liu**[1], **Dilip K. Deb**[1], **Lei He**[1], **Phillip J. Hsu**[4], **Tivoli Nguyen**[1], **Linda Zhang**[4], **Marc Bissonnette**[1], **Chuan He**[4,5], **Yan Chun Li**[1,6,*]

[1]Department of Medicine, Division of Biological Sciences, The University of Chicago, Chicago, Illinois, USA

[2]Institute of Biomedical Research, Shanxi Medical University, Taiyuan, Shanxi, China

[3]Department of Cardiology, Hainan General Hospital, Hainan Clinical Research Institute, Haikou, Hainan, China

[4]Departments of Chemistry, Biochemistry and Molecular Biology, The University of Chicago, Chicago, Illinois, USA

[5]Howard Hughes Medical Institute, The University of Chicago, Chicago, Illinois, USA

[6]Lead Contact

Summary

Bacterial infection triggers a cytokine storm that needs to be resolved to maintain the host's wellbeing. Here we report that ablation of m^{6}A methyltransferase subunit METTL14 in myeloid cells exacerbates macrophage responses to acute bacterial infection in mice, leading to high mortality due to sustained production of pro-inflammatory cytokines. METTL14 depletion blunts *Socs1* m^{6}A methylation and reduces YTHDF1 binding to the m^{6}A sites, which diminishes SOCS1 induction leading to overactivation of TLR4/NF- κB signaling. Forced expression of SOCS1 in macrophages depleted of METTL14 or YTHDF1 rescues the hyper-responsive phenotype of these macrophages *in vitro* and *in vivo*. We further show that LPS treatment induces *Socs1* m^{6}A methylation and sustains SOCS1 induction by promoting *Fto* mRNA degradation, and forced FTO expression in macrophages mimics the phenotype of METTL14-depleted macrophages. We conclude that m^{6}A methylation-mediated SOCS1 induction is required to maintain the negative feedback control of macrophage activation in response to bacterial infection.

*Correspondence: Yan Chun Li, cyan@medicine.bsd.uchicago.edu.

Author contributions

Conceptualization: Y.C.L.; Methodology and Investigation: J.D., W.L., W.L., D.K.D., P.H., L.H., T.N. and L.Z.; Formal analysis: J.D., W.L. and Y.C.L.; Writing – Original Draft: J.D. and Y.C.L.; Writing – Review & Editing: M.B., C.H., and Y.C.L.; Fund Acquisition: C.H., Y.C.L.; Resources: M.B.; Supervision: Y.C.L.

Declaration of interests

C.H. is a scientific founder and a member of the scientific advisory board of Accent Therapeutics, Inc. The other authors declare no competing interests.

eTOC Blurb

Bacterial infection triggers a cytokine storm that needs to be resolved to maintain the host's wellbeing, and the resolution relies on negative feedback loops to control cytokine production. Du et al. reveal a mechanism whereby m^{6}A-mediated induction of negative regulator SOCS1 controls macrophage activation in response to bacterial infection.

Graphical Abstract

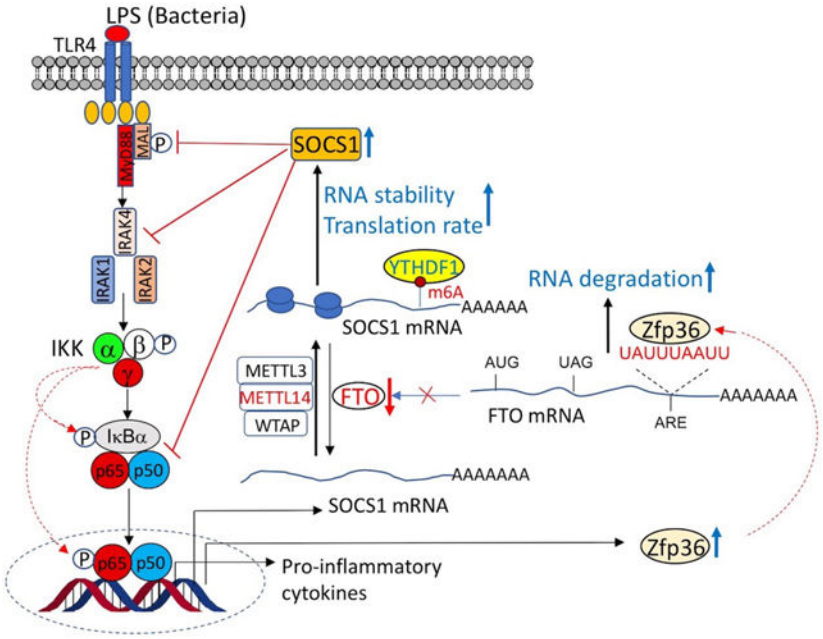

Keywords

m^{6}A methylation; METTL14; YTHDF1; FTO; SOCS1; Negative feedback; Macrophage; Cytokine storm; Bacterial infection; Sepsis

Introduction

Post-transcriptional modifications of RNAs have emerged as an essential regulatory mechanism controlling gene expression (Nachtergaele and He, 2017). *N*^{6}-adenosine methylation (m^{6}A) is the most abundant internal post-transcriptional modification in eukaryotic mRNAs, estimated to constitute ~0.4% of all adenosine nucleotides in RNAs from mammals (Wei, et al., 1975). The consensus motif for m^{6}A methylation is RRm^{6}ACH [(G/A/U)(G>A)m^{6}AC(U>A>C)] (Narayan and Rottman, 1988; Kane and Beemon, 1985), and m^{6}A methylation can occur in different regions of the mRNA transcript, with enrichment in long exons, near stop codons in 3'UTR and in 5'UTR regions surrounding the start codon (Zhou, et al., 2015a; Dominissini, et al., 2012).

Recent studies have demonstrated that m^{6}A mRNA methylation is reversible and dynamically regulated by writers, erasers and readers. Writers are methyl-transferases that

install the methyl group on adenosine residues, erasers are demethylases that remove the methyl group, and readers are proteins that recognize and interact with the m^6A site. The m^6A methyltransferase is a protein complex composed of methyltransferase-like 3 (METTL3), METTL14, Wilms tumor 1-associated protein (WTAP) and KIAA1429. Two m^6A erasers have been identified: fat mass and obesity-associated protein (FTO) and ALKBH5. The reader proteins include members of the YT521-B homology (YTH) domain-containing proteins (YTHDF1/2/3 and YTHDC1/2), the heterogeneous nuclear ribonucleoprotein (HNRNP) proteins (HNRNPA2B1 and HNRNPC) (Zhao, et al., 2017), and the insulin-like growth factor 2 mRNA-binding proteins (IGF2BP1/2/3) (Huang, et al., 2018). The readers mediate the functions of m^6A (Shi, et al., 2017; Alarcon, et al., 2015). For example, YTHDF1 controls mRNA degradation and increase translation efficiency (Wang, et al., 2015), YTHDF2 reduces target mRNA's half-life and promotes m^6A mRNA degradation (Du, et al., 2016; Wang, et al., 2014a), IGF2BPs promote mRNA stability and translation (Huang, et al., 2018), and YTHDC1 regulates chromatin state and transcription via interacting with m^6A sites on carRNAs (Liu, et al., 2020). Now it is recognized that m^6A methylation is a critical regulatory mechanism in genetic information flow that influences all fundamental aspects of mRNA metabolism, including mRNA processing, stability and translation (Zhao, et al., 2017), and thereby plays a variety of physiological roles. For example, m^6A methylation has been shown to determine stem cell fate and pluripotency (Cui, et al., 2017; Zhang, et al., 2017; Chen, et al., 2015; Geula, et al., 2015; Batista, et al., 2014; Wang, et al., 2014b), to control heat shock response (Zhou, et al., 2015a), to regulate hematopoietic progenitor differentiation (Lee, et al., 2019; Weng, et al., 2018), and to influence learning and memory (Koranda, et al., 2018; Shi, et al., 2018a).

Sepsis is a major clinical problem and leading cause of death in patients in intensive care units (ICU) worldwide (Angus and van der Poll, 2013). Sepsis, present in 6% of adult hospitalizations (Rhee, et al., 2017), is characterized by severe systemic inflammation and organ dysfunction as a result of dysregulated host responses to infection. Sepsis is usually caused by bacterial or viral infection that triggers a rapid cytokine storm, which is the host immune response to eliminate the infectious agent; however, excessive host response can lead to a deleterious and non-resolving systemic inflammatory response syndrome and organ failure (Vincent, et al., 2009). For example, sustained cytokine storm developed in severe COVID-19 patients is believed to be one of the most dangerous life-threatening events in the current COVID-19 pandemic (Coperchini, et al., 2020; Mahta, et al., 2020). Pro-inflammatory cytokines, such as IL-1α, IL-1β, IL-6 and TNF-α, play key roles in the development of sepsis (Chaudhry, et al., 2013). Macrophages as an essential component of innate immunity play a central role in the host defense against infection (Gordon and Martinez, 2010). Macrophages are a major cell type driving the cytokine storm during infection. As the first line of defense, activated macrophages release a plethora of pro-inflammatory cytokines and chemokines to initiate inflammatory response. To prevent overwhelming systemic inflammation, negative feedback mechanisms are in place to control the duration and intensity of the cytokine response. One of the most important negative feedback loops is controlled by the SOCS family of proteins (Duncan, et al., 2017; Yoshimura, et al., 2007), which are usually induced during inflammation. There are eight members of SOCS protein (CISH and SOCS1-7) that inhibit intracellular cytokine signaling

by binding to key signaling proteins through their Src-homology 2 (SH2) domain; meanwhile, their SOCS box promotes polyubiquitination and proteasomal degradation of the targeted signaling proteins (Yoshimura, et al., 2007).

To explore the role of m^{6}A methylation in macrophage activation in acute inflammatory response we have targeted METTL14, a key component of the m^{6}A methyltransferase, in myeloid cells. Our studies reveal critical roles of METTL14, YTHDF1 and FTO in the regulation of *Socs1* m^{6}A methylation that are required to maintain the negative feedback control of macrophage cytokine storm in acute bacterial infection.

Results

Myeloid cell-specific deletion of METTL14 renders mice hypersensitive to bacterial infection.

As global METTL14 ablation is lethal, we generated *Mettl14*$^{flox/flox}$ (designated as M14$^{f/f}$) mice that carry two LoxP sites flanking exons 7–9 in the *Mettl14* gene. To explore the function of METTL14 in macrophages, we crossed *Mettl14*$^{flox/flox}$ mice and LysM-Cre transgenic mice to generate *Mettl14*$^{flox/flox}$;LysM-Cre mice (designated as mM14$^{-/-}$) that carry *Mettl14* gene deletion in myeloid cells. LysM-Cre has been widely used to delete genes in monocytes and macrophages (Shi, et al., 2018b; Clausen, et al., 1999). Both male and female mM14$^{-/-}$ mice appeared normal with normal growth rate relative to M14$^{f/f}$ counterparts. We confirmed the depletion of METTL14 protein, but not METTL3 protein, in peritoneal macrophages and bone marrow derived macrophages (BMDMs) isolated from mM14$^{-/-}$ mice (Figure S1A). Consistently, RNA m^{6}A methylation, detected by anti-m^{6}A antibody, was dramatically reduced in mM14$^{-/-}$ BMDMs with or without LPS stimulation (Figure S1B). We first studied mM14$^{-/-}$ mice using the cecum ligation and puncture (CLP) model. This model is the most stringent sepsis model consisting of perforation of the cecum, which allows the release of fecal materials into the peritoneal cavity to generate an exacerbated immune response induced by polymicrobial infection. This model mimics many aspects of human sepsis and is the most widely utilized sepsis model for human acute lung injury and acute respiratory distress syndrome (Dejager, et al., 2011). After CLP surgery (Toscano, et al., 2011), mM14$^{-/-}$ mice developed more severe symptom of sepsis compared with M14$^{f/f}$ littermates. By 65 hours 50% mM14$^{-/-}$ mice had died, whereas only 15% M14$^{f/f}$ mice were dead (Figure S1C). Peritoneal macrophages freshly isolated from mM14$^{-/-}$ mice at 24 hours after CLP surgery showed much greater induction of pro-inflammatory cytokine (*Tnfa, Il1b, Il6, Ifng, Il17*), *Tlr4* and *Cd14* transcripts compared to M14$^{f/f}$ counterparts (Figure S1D). Serum concentrations of pro-inflammatory cytokines (TNF-α, IL-1β, IL-6 and IFN-γ) in mM14$^{-/-}$ mice were much higher compared to M14$^{f/f}$ mice (Figure S1E). Consistently, mM14$^{-/-}$ mice showed more severe lung injury, with greater increases in alveolar wall thickness and immune cell infiltration (Figure S1F) and in myeloperoxidase (MPO) activity in lung lysates compared to M14$^{f/f}$ mice (Figure S1G).

We further examined these mice using the lipopolysaccharide (LPS)-induced sepsis model. LPS is a Gram-negative bacterial endotoxin that induces septic shock in the host via Toll-like receptor 4 (TLR4) /CD14 (Raetz and Whitfield, 2002). LPS administration causes severe systemic inflammation and is widely used to induce acute sepsis. Following LPS

injection, all mM14$^{-/-}$ mice died within 48 hours, whereas 80% M14$^{f/f}$ mice survived >120 hours (Fig. 1A). Similar to the CLP model, LPS induced more severe lung injury in mM14$^{-/-}$ mice than in M14$^{f/f}$ mice (Fig. 1B). mM14$^{-/-}$ peritoneal macrophages freshly isolated at 24 hours after LPS challenge showed much more robust induction of pro-inflammatory cytokine (*Tnfa, Il1b, Il6, Ifng, and Il17*), *Tlr4* and *Cd14* transcripts compared with M14$^{f/f}$ counterparts (Fig. 1C), and serum pro-inflammatory cytokine (TNF-α, IL-1β, IL-6 and IFN-γ) concentrations were much more elevated in mM14$^{-/-}$ mice than in M14$^{f/f}$ mice after LPS stimulation (Fig. 1D). The data from both CLP and LPS sepsis models suggest that mM14$^{-/-}$ mice most likely succumbed from excessive and non-resolving systemic inflammation.

Macrophages depleted of METTL14 are hyper inflammatory.

As LysM-Cre is broadly expressed in myeloid cells, we set out to directly assess the inflammatory response in cultured macrophages derived from M14$^{f/f}$ and mM14$^{-/-}$ mice. For either peritoneal macrophages (Fig. 1E) or BMDMs (Fig. 1F), the induction of pro-inflammatory cytokines and chemokines (*Tnfa, Il1b, Il6, Cxcl2*) was much more robust in mM14$^{-/-}$cells compared with M14$^{f/f}$ cells following LPS stimulation; however, after the induction peaked, all cytokines declined at a much slower pace in mM14$^{-/-}$ macrophages (Fig. 1E, F), suggesting a dysregulation of the intensity and duration of inflammatory responses in the mutant cells. Consistently, the amount of pro-inflammatory cytokines (TNF-α, IL-1β, IL-6 and IFN-γ) secreted into the media from LPS-activated mM14$^{-/-}$ BMDMs was much greater compared to M14$^{f/f}$ counterparts (Fig. 1G). These data confirm that METTL14 depletion renders macrophages hyperactive in pro-inflammatory cytokine induction in response to LPS stimulation.

As both CLP and LPS sepsis models are mediated by TLR4, we also examined TLR3-mediated responses in M14$^{f/f}$ and mM14$^{-/-}$ mice using poly(I:C) challenge. Poly(I:C) mimics double-stranded virus infection and stimulates macrophages via TLR3 (Fortier, et al., 2004). Poly(I:C) administration markedly increased serum pro-inflammatory cytokine concentrations in both M14$^{f/f}$ and mM14$^{-/-}$ mice (Figure S2A), and stimulated *Tlr3, Tnfa, Il1b, Il6* and *Ifng* expression in peritoneal macrophages in these mice (Figure S2B), but there were no differences in cytokine induction between these two genotypes. Therefore, *Mettl14* deletion appears to specially impair TLR4-mediated pathways in macrophage activation. We further analyzed M14$^{f/f}$ and mM14$^{-/-}$ BMDMs in culture. Again, poly(I:C) stimulation led to marked increases in cytokine transcripts (Figure S2C) as well as in cytokine secretions (Figure S2D), but again no differences were seen between these two types of cells. As such, we focused on TLR4-mediated pathways in the following investigations.

Hyper inflammatory response is of hematopoietic origin.

To confirm that the severe septic response of mM14$^{-/-}$ mice is caused by defects in hematopoietic cells, we performed bone marrow (BM) transplantation (BMT) and analyzed the recipient mice eight weeks after BMT. As shown in Figure S3, in either the control BMT experiment where donor BM cells were transplanted to recipients of the same genotype (M14$^{f/f}$ BM > M14$^{f/f}$ mice; mM14$^{-/-}$ BM > mM14$^{-/-}$ mice), or in the cross BMT experiment where donor BM cells were transplanted to recipients with the opposite

genotype ($M14^{f/f}$ BM > $mM14^{-/-}$ mice; $mM14^{-/-}$ BM > $M14^{f/f}$ mice), the sepsis phenotype of the recipient mice was determined by the donor BM genotype, not by the recipient mouse genotype. That is, regardless of the recipient's genotype, following LPS challenge, mice receiving $mM14^{-/-}$ BM cells died faster with 100% mortality within 36 hours (Figure S3A and B), exhibited much higher levels of serum pro-inflammatory cytokines (Figure S3C and D), and their peritoneal macrophages showed much more robust induction of pro-inflammatory cytokines (TNF-α, IL-1β, IL-6 and IFN-γ) (Figure S3E and F), compared with mice receiving $M14^{f/f}$ BM cells. These observations confirm that BM-derived hematopoietic cells are the origin of the hyper-responsive macrophages in $mM14^{-/-}$ mice.

Macrophage genotypes determine mouse inflammatory response.

To demonstrate that $mM14^{-/-}$ macrophages are the cause of the severe septic response seen *in vivo*, we performed macrophage depletion/reconstitution experiments. We depleted macrophages using clodronate-containing liposomes (Weisser, et al., 2012), a method specific for macrophage depletion, as macrophages undergo apoptosis upon phagocytosis of clodronate liposomes (Naito, et al., 1996; van Rooijen, et al., 1996). Intravenous administration of one dose of clodronate-liposomes was able to eliminate >99% $F4/80^{+}MHCII^{+}$ macrophages in the spleen within 48 hrs (Figure S4A and B), and peritoneal macrophages could not be obtained at this time. Two days after clodronate-liposome treatment, we reconstituted the depleted mice with fully differentiated BMDMs by intravenous injection. Then 36 hours after the reconstitution, we challenged the reconstituted mice with LPS. In either the parallel reconstitution where BMDMs were injected to recipients with the same genotype ($M14^{f/f}$ BMDM > $M14^{f/f}$ mice; $mM14^{-/-}$ BMDM > $mM14^{-/-}$ mice), or in the cross reconstitution where BMDMs were transferred to recipients with the opposite genotype ($M14^{f/f}$ BMDM > $mM14^{-/-}$ mice; $mM14^{-/-}$ BMDM > $M14^{f/f}$ mice), the septic phenotype of the recipient mice was determined by the genotype of the reconstituted donor BMDMs, not by the genotype of the recipient mouse. That is, regardless of the recipient's genotype, following LPS challenge depleted mice receiving $mM14^{-/-}$ BMDMs died faster with 100% mortality by 36 hrs (Figure S4C and D), had much higher levels of serum pro-inflammatory cytokines (Figure S4E and F), and their peritoneal macrophages showed more robust induction of pro-inflammatory cytokines (TNF-α, IL-1β, IL-6 and IFN-γ) compared with depleted mice receiving $M14^{f/f}$ BMDMs (Figure S4G and H). Control liposome treatment did not alter the inflammatory phenotype of the mice. These observations confirm that mutant macrophages are the cause of the severe septic response seen in $mM14^{-/-}$ mice.

SOCS1 is a METTL14 target to control macrophage activation.

As m^6A methylation directly controls the status of mRNA transcripts, the primary cause for $mM14^{-/-}$ macrophage dysfunction should lie in macrophage mRNAs. To identify macrophage mRNA transcripts whose expressions are affected by METTL14 deletion, we profiled the m^6A epitranscriptome and transcriptome of $M14^{f/f}$ and $mM14^{-/-}$ macrophages at baseline and under LPS stimulation, and then correlated the m^6A methylation and RNA expression profiles through integrated analyses of these two datasets. Specifically, we performed m^6A RNA-IP-seq (RIP-seq) (Dominissini, et al., 2013) and RNA-seq (Mortazavi, et al., 2008) using poly(A^{+}) RNAs isolated from PBS- (Control) or LPS-treated $M14^{f/f}$ and

mM14$^{-/-}$ BMDMs, and each experimental group contained BMDMs derived from three independent mice.

The RIP-seq data showed that m^{6}A peaks are enriched near the stop codon in 3'-UTR (FDR-corrected p< 0.01), and the peak motif is 5'-G(A)G(A)ACU(A)-3' (p=1.0×10^{-126}) in all experimental groups (Fig. 2A), consistent with the known consensus m^{6}A methylation motif (Narayan and Rottman, 1988; Kane and Beemon, 1985). Cumulative fraction data suggest that marked differences between M14$^{f/f}$ and mM14$^{-/-}$ m^{6}A peaks occurs in the peaks highly suppressed by LPS (Log$_2$FC<−2.5) (Fig. 2B). LPS induced 442 m^{6}A peaks in M14$^{f/f}$ BMDMs and 405 peaks in mM14$^{-/-}$ BMDMs, among which 324 peaks are common for M14$^{f/f}$ and mM14$^{-/-}$ cells (Log$_2$FC>0, FDR p<0.05). On the other hand, LPS lowered 2,064 m^{6}A peaks in M14$^{f/f}$ BMDMs and 1,736 peaks in mM14$^{-/-}$ BMDMs, among which 1,244 peaks are common in both M14$^{f/f}$ and mM14$^{-/-}$ cells (Log$_2$FC<0, FDR p<0.05). Of particular interest are 1,796 peaks that were altered (increased or decreased) by LPS in M14$^{f/f}$ BMDMs but were absent in mM14$^{-/-}$ cells, and we speculated that these M14$^{f/f}$-unique m^{6}A peaks are most likely associated with authentic METTL14-targeted transcripts under LPS challenge (Fig. 2C).

In RNA-seq analyses, LPS treatment upregulated 3,224 genes in M14$^{f/f}$ BMDMs and 3,460 genes in mM14$^{-/-}$ BMDMs, among which 2,431 genes were common to both M14$^{f/f}$ and mM14$^{-/-}$ cells (FC>1.5, FDR p<0.05). On the other hand, LPS down-regulated 3,760 genes in M14$^{f/f}$ BMDMs and 3,565 genes in mM14$^{-/-}$ BMDMs, among which 2,785 genes were common to M14$^{f/f}$ and mM14$^{-/-}$ cells (FC<−1.5, FDR p<0.05) (Fig. 2D, E and F). Cumulative fraction data suggest that the largest differences are found in LPS-suppressed transcripts (including both m^{6}A-methylated and unmethylated transcripts) between M14$^{f/f}$ and mM14$^{-/-}$ cells (Fig. 2G).

To search for METTL14-targeted transcripts, we reasoned that the direct, most biologically meaningful METTL14 targets were those whose m^{6}A methylation was depleted or markedly diminished while their expression was altered, positively or negatively, in mM14$^{-/-}$ cells. Therefore, we correlated the 1,454 transcripts associated with the M14$^{f/f}$-unique m^{6}A peaks from the RIP-seq datasets with the 2,876 transcripts from the RNA-seq datasets whose expression was significantly increased or decreased (0<Log$_2$FC<0, FDR p<0.05) in mM14$^{-/-}$ cells relative to M14$^{f/f}$ cells in response to LPS treatment, and found 356 overlapped mRNA transcripts (Fig. 2H). Figure 2I shows the top 20 LPS-induced m^{6}A peaks (according to LPS-induced log$_2$FC) and the corresponding mRNA transcripts, and *Socs1* transcript is among the top 10 whose log$_2$LPS-induced FC was reduced by about 2-fold in mM14$^{-/-}$ BMDMs compared with M14$^{f/f}$ BMDMs (Fig. 2I).

We also examined the other members of the SOCS family. *Socs2* transcript was not m^{6}A-methylated. Although *Socs3* transcript was heavily m^{6}A-methylated and the methylation was induced by LPS, METTL14 depletion had little effects on the methylation or the induction of *Socs3* transcript under LPS or CLP challenge (Figure S5A–C). The moderate methylation of *Socs4*, *Socs5* and *Socs6* transcripts was suppressed (rather induced) by LPS, and METTL14 depletion had little effects on these transcripts under LPS or CLP challenge (Figure S5A–C). *Socs7* and *Cish* m^{6}A methylation was not altered by LPS or METTL14

depletion, and METTL14 deletion had little and inconsistent effects on the induction of these transcripts under LPS or CLP challenge (Figure S5A–C). Therefore, except for SOCS1, all the other SOCS mRNAs do not fit the definition of direct METTL14 target. Therefore, given the critical role of SOCS1 in the negative feedback regulation of LPS/TLR4 signaling (Nakagawa, et al., 2002; Marine, et al., 1999), we focused on SOCS1 as a top candidate METTL14 target in sepsis, because a defective negative feedback loop well explains the uncontrolled and overactivated phenotype of mM14$^{-/-}$ macrophages.

Socs1 m^{6}A methylation is required to maintain SOCS1-mediated negative feedback control.

Examination of the read density confirmed that LPS dramatically induced m^{6}A methylation on *Socs1* transcript in M14$^{f/f}$ BMDMs, but the effect of LPS on *Socs1* mRNA in mM14$^{-/-}$ cells was markedly diminished (Fig. 3A). LPS induced 4 major m^{6}A peaks throughout the *Socs1* transcript, one in 3'UTR (site 1), one near the stop codon (site 2) and two in the coding region (sites 3 and 6) (Fig. 3A). We confirmed by m^{6}A RIP-qPCR that LPS indeed induced *Socs1* m^{6}A methylation in M14$^{f/f}$ BMDMs at sites 1, 2, 3 and 6, but not at sites 4 and 5, and these inductions were significantly diminished in mM14$^{-/-}$ cells (Fig. 3B). We also confirmed in time course studies that LPS markedly induced *Socs1* mRNA and SOCS1 protein in cultured M14$^{f/f}$ BMDMs and peritoneal macrophages, peaking at around 4 hrs, but these inductions were clearly attenuated in mM14$^{-/-}$ cells (Fig. 3C, D and E). Consistently, impaired SOCS1 induction was also seen *in vivo*, as the induction of *Socs1* transcript was markedly attenuated in peritoneal macrophages freshly isolated from mM14$^{-/-}$ mice at 12 and 24 hrs after LPS challenge (Fig. 3F), or from mM14$^{-/-}$ mice following CLP (Fig. 3G), compared with M14$^{f/f}$ counterparts. The same is also true for peritoneal macrophages freshly isolated from LPS-treated recipient mice that were transplanted with mM14$^{-/-}$ BM compared with mice transplanted with M14$^{f/f}$ BM (Fig. 3H), or from LPS-treated macrophage-depleted mice reconstituted with mM14$^{-/-}$ BMDMs verse mice reconstituted with M14$^{f/f}$ BMDMs (Fig. 3I), as described in Figure S3 and S4. NF-κB signaling pathway is a final common pathway of TLR-mediated immune response that is negatively regulated by SOCS1 (Yoshimura, et al., 2007; Liew, et al., 2005; Beutler, 2004). Because of the impaired induction of SOCS1, the activation of NF-κB signaling was much more robust in mM14$^{-/-}$ BMDMs upon LPS stimulation compared with M14$^{f/f}$ cells, which was reflected by more robust phosphorylation of IKKα/β and p65 and more dramatic degradation of IκBα at 1 hour following LPS treatment (Fig. 3J). To address whether the lack of m^{6}A methylation in *Socs1* mRNA reduced SOCS1 translation, we pulse-labelled newly translated SOCS1 protein with L-azidohomoalanine (AHA) in M14$^{f/f}$ and mM14$^{-/-}$ BMDMs treated with PBS or LPS. Whereas LPS dramatically induced new SOCS1 synthesis revealed by one-hour AHA pulse labelling in M14$^{f/f}$ cells, newly translated SOCS1 was barely detectable in LPS-treated mM14$^{-/-}$ BMDMs even after two hours of AHA labelling (Fig. 3K), indicating that m^{6}A methylation is indeed required for the translation of new SOCS1 protein under LPS challenge. Consistently, at the PBS control baseline, newly translated SOCS1 was only detectable after two-hour AHA labelling in M14$^{f/f}$ cells but not in mM14$^{-/-}$ cells (Fig. 3K). Collectively, these observations demonstrate that *Socs1* m^{6}A methylation is required to maintain the SOCS-1 mediated negative feedback loop in macrophage activation.

YTHDF1 is the reader to control SOCS1 induction.

Next we performed cross-linking and RNA immunoprecipitation (CLIP) assays (Weng, et al., 2018) to search for the reader(s) that interact with *Socs1* m^{6}A sites in macrophages. In RAW264.7 macrophages we confirmed that *Socs1* m^{6}A sites 1, 2, 3 and 6 interact with writers METTL3 and METTL14 as expected (Fig. 4A); we also surveyed all known m^{6}A readers (IGF2BP1/2/3, YTHDC1/2, or YTHDF1/2/3) and found only YTHDF1 binds to sites 2, 3 and 6 (Fig. 4B). We confirmed that in BMDMs METTL3 and METTL14 bind to sites 1, 2, 3 and 6, and YTHDF1 binds to sites 2, 3 and 6, but all these interactions were dramatically diminished in mM14$^{-/-}$ BMDMs (Fig.4C). This is because METTL14 deletion reduces m^{6}A methylation, which depletes the binding site for YTHDF1. These observations demonstrate that YTHDF1 is the reader for *Socs1* m^{6}A sites. As YTHDF1 acts to increase mRNA stability and translation efficiency (Wang, et al., 2015), it is reasonable to speculate that impaired SOCS1 induction seen in mM14$^{-/-}$ cells is largely due to the lack of YTHDF1-mediated translation.

To functionally validate the role of the METTL14-YTHDF1-SOCS1 axis in macrophage activation, we then studied *Ythdf1*$^{-/-}$ mice (Shi, et al., 2018a) using both CLP- and LPS-induced sepsis models. We reasoned that, if YTHDF1 is the reader that mediates the biological activities of *Socs1* m^{6}A sites, then YTHDF1 deletion should phenocopy METTL14 deletion in macrophage septic responses. *Ythdf1*$^{-/-}$ mice appeared normal at baseline. After CLP surgery, 90% *Ythdf1*$^{-/-}$ mice died by 96 hrs, whereas only 30% wild-type (WT) littermates died (Fig. 4D). At 24 hrs after CLP surgery, peritoneal macrophages freshly isolated from *Ythdf1*$^{-/-}$ mice exhibited much greater induction of pro-inflammatory cytokines (*Tnfa, Il1b, Il6, Ifng*) than WT counterparts (Fig. 4E). Similarly, following LPS challenge all *Ythdf1*$^{-/-}$ mice died within 24 hrs, whereas only 40% WT mice died before 48 hrs (Fig. 4F), and *Ythdf1*$^{-/-}$ peritoneal macrophages isolated at 24 hrs produced much higher pro-inflammatory cytokines than WT peritoneal macrophages (Fig. 4G). *In vitro* BMDM cultures confirmed more robust and lasting pro-inflammatory cytokine production in *Ythdf1*$^{-/-}$ BMDMs following LPS stimulation (Fig. 4H and I). Importantly, the induction of *Socs1* mRNA was markedly attenuated in *Ythdf1*$^{-/-}$ peritoneal macrophages freshly isolated from either CLP-treated or LPS-treated mice (Fig. 4E and G), as well as in LPS-stimulated *Ythdf1*$^{-/-}$ BMDMs (Fig. 4J). Similarly, the induction of SOCS1 protein by LPS was impaired in *Ythdf1*$^{-/-}$ BMDMs compared with WT BMDMs (Fig. 4K), which is more clearly illustrated by a time course study (Fig. 4L). Similar as seen in mM14$^{-/-}$ BMDMs, because of the defective SOCS1 induction, the activation of NF-κB signaling was more robust in *Ythdf1*$^{-/-}$ BMDMs upon LPS stimulation compared with WT BMDMs, reflected by more robust phosphorylation of IKKα/β and p65 and more dramatic degradation of IκBα at 60 min (Fig. 4M). Also similar as seen in mM14$^{-/-}$ BMDMs, newly translated SOCS1 protein induced by LPS was barely detectable in *Ythdf1*$^{-/-}$ BMDMs even after two-hour AHA pulse labelling (Fig. 4N), indicating that the interaction of YTHDF1 with m^{6}A on *Socs1* mRNA is crucial for new SOCS1 protein translation under LPS challenge. Taken together, these observations demonstrate that YTHDF1 is the *Socs1* m^{6}A reader required for proper induction of macrophage SOCS1 in septic responses.

SOCS1 rescues macrophage defects caused by METTL14 or YTHDF1 deletion.

To functionally demonstrate that SOCS1 acts downstream of METTL14 or YTHDF1 to regulate macrophage activation, we assessed the *in vitro* and *in vivo* effects of lentivirus-mediated forced SOCS1 expression in mM14$^{-/-}$ or *Ythdf1*$^{-/-}$ macrophages. As expected, when mM14$^{-/-}$ BMDMs were transduced with METTL14-lentivirus, not only METTL14 expression was restored, but the induction of SOCS1 under LPS stimulation was also markedly elevated compared with mM14$^{-/-}$ BMDMs infected with empty control lentivirus (Fig. 5A). Also as expected, the induction of pro-inflammatory cytokines (*Tnfa, Il1b, Il6, Ifng, Il17*) by LPS was alleviated in METTL14-lentivirus infected mM14$^{-/-}$ BMDMs and normalized to the levels seen in control virus-infected M14$^{f/f}$ BMDMs (Fig. 5B). Importantly, when mM14$^{-/-}$ BMDMs were transduced with SOCS1-lentivirus (Fig. 5A), LPS-induced pro-inflammatory cytokines were also normalized to the levels of control virus-infected M14$^{f/f}$ BMDMs (Fig. 5B). In similar experiments, we found that *Ythdf1*$^{-/-}$ BMDMs transduced with SOCS1-lentivirus (Fig. 5C) were much less inflammatory compared with *Ythdf1*$^{-/-}$ BMDMs infected with control lentivirus, with a marked reduction in the production of these pro-inflammatory cytokines following LPS stimulation, and the cytokine levels were normalized to those seen in control virus-transduced WT BMDMs (Fig. 5D).

We then performed macrophage depletion/reconstitution experiments to demonstrate the rescue of the hyperinflammatory abnormalities of mM14$^{-/-}$ or *Ythdf1*$^{-/-}$ macrophages *in vivo* (Fig. 5E). Clodronate-treated, macrophage-depleted mice reconstituted with control virus-infected mM14$^{-/-}$ BMDMs showed 100% mortality within 36 hours after LPS challenge, whereas reconstitution with METTL14-lentivirus-transduced mM14$^{-/-}$ BMDMs markedly reduced the mortality (Fig. 5F) and the levels of serum pro-inflammatory cytokines (Fig. 5G); importantly, reconstitution with SOCS1-lentivirus-infected mM14$^{-/-}$BMDMs was also able to markedly improve the survival following LPS challenge and reduce serum pro-inflammatory cytokines to the levels seen in mice reconstituted with control-virus-transduced M14$^{f/f}$ BMDMs (Fig. 5F and G). Similarly, we observed a marked improvement in survival (Fig. 5H) and a substantial reduction in serum pro-inflammatory cytokines (Fig. 5I) in macrophage-depleted mice reconstituted with SOCS1-lentivirus infected *Ythdf1*$^{-/-}$ BMDMs, in comparison with the reconstitution with control lentivirus-infected *Ythdf1*$^{-/-}$ BMDMs, which showed 100% mortality within 24 hours following LPS challenge (Fig. 5H). Again, the serum cytokine levels in the mice reconstituted with SOCS1-lentivirus infected YTHDF1$^{-/-}$ BMDMs were normalized to the levels seen in mice reconstituted with control-virus-transduced WT BMDMs (Fig. 5I). Therefore, forced expression of SOCS1 was also able to completely correct the hyper-inflammatory phenotype of mM14$^{-/-}$ and *Ythdf1*$^{-/-}$ macrophages *in vitro* and *in vivo*. Together these data demonstrate a key role of the METTL14-YTHDF1-SOCS1 axis in the control of macrophage activation in response to TLR4-mediated bacterial infection.

FTO is the eraser to regulate *SOCS1* m^{6}A methylation in macrophage activation.

Our RIP-seq data showed that *Socs1* m^{6}A methylation is induced during macrophage activation. We demonstrated that this increase in methylation is required to sustain SOCS1 levels to maintain a proper negative control in septic response. The global m^{6}A methylation

in macrophages is in fact induced in response to LPS challenge (see Fig. S1B). We confirmed by ELISA quantitation that m^{6}A induction occurred not only in cultured BMDMs, but also in peritoneal macrophages freshly isolated from CLP- or LPS-treated mice (Fig. 6A), indicating that m^{6}A induction is an *in vivo* physiological phenomenon. To address whether the m^{6}A induction is related to m^{6}A erasers, we quantified ALKBH5 and FTO, two known m^{6}A demethylases, in macrophages under LPS stimulation. In RAW264.7 macrophages LPS had no effects on *ALKBH5* expression, but clearly suppressed FTO at both the mRNA and protein levels in a time-dependent manner (Fig. 6B and C). This observation offers an explanation why *Socs1* m^{6}A methylation is increased in LPS-induced macrophages activation. To directly assess the relationship between FTO and SOCS1, we overexpressed FTO in RAW264.7 cells via lentiviral transduction (Fig. 6D). As expected, forced FTO expression suppressed the global m^{6}A methylation at baseline and under LPS stimulation (Fig. 6E); importantly, LPS-induced m^{6}A methylations throughout the *Socs1* transcript were also suppressed (Fig. 6F). Consistent with the decrease in m^{6}A methylation, CLIP assays revealed that FTO overexpression drastically suppressed YTHDF1 binding to m^{6}A sites 2, 3 and 6 on the *Socs1* transcript (Fig. 6G). Furthermore, forced FTO expression markedly blocked SOCS1 induction in LPS-treated macrophages (Fig. 6D). These observations indicate that FTO directly regulates SOCS1 by removing the m^{6}A methyl groups on *Socs1* mRNA.

To functionally link FTO to macrophage activation, we transduced WT BMDMs with FTO-expressing lentivirus or empty control lentivirus. As expected, FTO-expressing BMDMs exhibited more robust induction of pro-inflammatory cytokine transcripts (*Tnfa, Il1b, Il6, Ifng, Il17*) upon LPS stimulation compared with BMDMs transduced with control lentivirus (Fig. 6H). Moreover, macrophage-depleted mice that were reconstituted with BMDMs transduced with FTO-lentivirus exhibited much greater mortality (100% mortality within 36 hours) (Fig. 6I) and much higher concentrations of serum pro-inflammatory cytokines (Fig. 6J) following LPS challenge, compared with the reconstitution with control virus-infected BMDMs. These observations indicate that FTO overexpression phenocopies METTL14 deletion in macrophage activation via SOCS1 regulation, consistent with the notion that the induction of *Socs1* m^{6}A methylation is required for the negative feedback control of macrophage activation.

We further examined the effects of LPS on the expression of m^{6}A writers (METTL14, METTL3, WTAP), erasers (FTO, ALKBH5) and readers (YTHDF1/2/3, YTHDC1/2, HNRNPA2B1, HNRNPC, IGF2BP1/2/3) in macrophages. As shown in Figure S6, except for *Mettl14*, METTL14 depletion had no significant effects on the expression of these writers, erasers and readers, and except for *Fto*, LPS treatment had no significant effects on these writers, erasers and readers in M14$^{f/f}$ and mM14$^{-/-}$ BMDMs (Figure S6A and B). Therefore, a potential LPS regulation of these m^{6}A writers and readers is unlikely accountable for the changes in *Socs1* mRNA methylation and expression.

Zfp36 promotes *Fto* mRNA degradation in macrophage activation.

Our data indicate that FTO down-regulation is crucial for the induction of *Socs1* m^{6}A methylation in macrophage activation, which leads to increased SOCS1 translation to sustain

the negative feedback loop. We found that FTO mRNA rapidly decayed in macrophages following LPS challenge (Fig. 7A). Degradation of mRNAs is a major mechanism to control gene expression (Guhaniyogi and Brewer, 2001). Interestingly, in the long 3'UTR of *Fto* mRNA we identified a highly conserved AU-rich element (ARE) (UAUUUAAUU) at nucleotide (nt) 3148 (Fig. 7B). It is well established that such an ARE mediates rapid RNA degradation when it interacts with a RNA binding protein (Bolognani and Perrone-Bizzozero, 2008; Winstall, et al., 1995; Shaw and Kamen, 1986). The group of ARE-binding proteins that destabilize mRNAs include HNRNPD/AUF1, Zfp36/TTP, BRF1, TIA-1, TIAL1/TIAR and KHSRP/KSRP (Bolognani and Perrone-Bizzozero, 2008). As LPS treatment decreased *Fto* mRNA in macrophages, we reasoned that an ARE-binding protein that mediates *Fto* mRNA degradation should be up-regulated by LPS. We therefore surveyed our BMDM RNA-seq database and found that, among HNRNPD, Zfp36, BRF1, TIA-1, TIAL1 and KHSRP, only Zfp36 is markedly up-regulated in LPS-treated BMDMs (Fig. 7C), and we validated this finding in LPS-treated RAW264.7 macrophages by RT-qPCR quantitation of these transcripts and a time-course Western blotting analysis of Zfp36 protein (Fig. 7D and E). Zfp36 is known to interact with a protein complex to exert its RNA degrading activity (Tiedje, et al., 2010). We confirmed by CLIP-qPCR assays that LPS indeed markedly increases Zfp36 binding to the ARE region within *Fto* mRNA 3'UTR (Fig. 7F).

To validate the activity of Zfp36-ARE interaction in mRNA degradation, we performed luciferase reporter assays. In HEK293 cells co-transfected with pRP-mZfp36 and pGL3-FTOARE that carries the *Fto* 3'UTR ARE(nt3148) (Fig. 7G), luciferase activity was dramatically suppressed (Fig. 7H); however, no suppression in luciferase activity was seen in co-transfection with pRP-mZfp36 and pGL3-FTOAREmut that carries a mutant ARE(nt3148) (5'UAAAAAAUU3'), or with pRL-CMV empty plasmid and pGL3-FTOARE (Fig. 7G and H). Together these observations confirm that Zfp36 promotes *Fto* mRNA degradation via interacting with the ARE within *Fto* 3'UTR to control macrophage activation.

Discussion

Sepsis is a life-threatening disease characterized by overwhelming systemic inflammation and organ dysfunction caused by a dysregulated host response to infection. Macrophages as key effectors of innate immunity play an essential role in host defense against microorganism infection. After infection, innate immune cells sense the pathogens by recognizing pathogen-associated molecular patterns (PAMPs) through an assortment of cell-surface and intracellular pattern recognition receptors (PRRs) including TLRs (Liew, et al., 2005). PPRs interact with diverse PAMPs to trigger the activation of downstream signaling pathways that are responsible for a burst of production of pro-inflammatory cytokines and chemokines. The rapidly increased inflammatory factors, named cytokine storm, recruit leukocytes and activate the complement and coagulation systems to eliminate the pathogens (van der Poll, et al., 2017). However, excessive, over-sustained inflammatory responses can trigger a systemic inflammatory response syndrome (Vincent, et al., 2009). The NF-κB pathway is a common signaling pathway activated by TLRs that stimulates the transcription of numerous pro-inflammatory mediators (Beutler, 2004). In sepsis, an excessive and un-

resolved cytokine storm causes cellular injury that results in the release of damage-associated molecular patterns (DAMPs), which further activate PRRs to initiate a vicious cycle, leading to organ damage, catabolism and death (van der Poll, et al., 2017). There are numerous negative regulatory mechanisms designed to prevent an excessive and fatal systemic inflammation or to ensure TLR tolerance (Yoshimura, et al., 2007; Liew, et al., 2005). For the TLR4/NF-κB signaling pathway that mediates inflammation from Gram-negative bacterial infection, a number of negative intracellular regulators have been identified at multiple levels that are induced by LPS through a negative feedback mechanism. These include A20 (Boone, et al., 2004), IRAKM (Kobayashi, et al., 2002), ST2 (Brint, et al., 2004), MyD88s (Janssens, et al., 2002) and SOCS1 (Kinjyo, et al., 2002; Nakagawa, et al., 2002).

SOCS1 is a central negative regulator of TLR4 signaling. Forced SOCS1 expression in macrophages inhibits LPS-induced NF-κB activation. Mice depleted of *Socs1* gene are hyper responsive to LPS challenge resulting in extremely high mortality, and SOCS1-deficient macrophages are hyper-activated with overproduction of pro-inflammatory cytokines upon LPS treatment (Kinjyo, et al., 2002; Nakagawa, et al., 2002). SOCS1 is known to suppress the TLR4/NF-κB signaling pathway at multiple sites. Mal (also called TIRAP) is a TIR-domain-containing adaptor protein that interacts with MyD88 and TRAF6 to transduce TLR4 signals to activate NF-κB (Verstak, et al., 2009; Kawai and Akira, 2007; Kagan and Medzhitov, 2006; Mansell, et al., 2004) and thus is critical for TLR4-mediated inflammatory response. SOCS1 binds to tyrosine-phosphorylated Mal via its SH2 domain and acts as an E3 ubiquitin ligase via its SOCS domain to drive Mal polyubiquitination and degradation (Yoshimura, et al., 2007; Mansell, et al., 2006). By similar mechanism SOCS1 interacts with p65 subunit of NF-κB to induces p65 degradation (Strebovsky, et al., 2011; Ryo, et al., 2003). There is evidence that SOCS1 also ubiquitinates and degrades TRAF6 (Zhou, et al., 2015b). Moreover, SOCS1 directly targets JAK. It blocks LPS-induced IL-6 production by disrupting JAK2-STAT5 signaling (Kimura, et al., 2005), and inhibits LPS-induced, IFN-β-dependent secondary activation of JAK-STAT1 signaling in innate immunity (Baetz, et al., 2004).

Given its importance in inflammatory regulation, SOCS1 is tightly controlled by multiple mechanisms to ensure a proper level under various circumstances. SOCS1 was first cloned as a JAK-binding cytokine signaling inhibitors (Endo, et al., 1997; Naka, et al., 1997; Starr, et al., 1997). Indeed, as the central molecule in the negative feedback loop in cytokine signaling, SOCS1 expression is highly induced by the JAK-STAT pathway (Krebs and Hilton, 2000). In septic response, SOCS1 is rapidly induced by LPS or bacterial infection (Kinjyo, et al., 2002; Nakagawa, et al., 2002), but how the LPS/TLR4 signaling up-regulates SOCS1 expression remains unclear. We observed that *Socs1* transcript induction lags the induction of cytokines in LPS-treated macrophages by several hours. Thus, SOCS1 might be secondarily induced by LPS-induced cytokines via the JAK-STAT pathway. Studies from SOCS1-deficient mice indicate that SOCS1 induction is essential to maintain a balanced septic response to prevent excessive harm to the host. On the other hand, SOCS1 is negatively regulated by miR-155 (Lu, et al., 2015; Chen, et al., 2013; Wang, et al., 2010), which itself is strongly induced by LPS/TLR4 signaling in macrophages to maximize the inflammatory process (Ruggiero, et al., 2009; O'Connell, et al., 2007).

In this study we identified a novel mechanism of SOCS1 regulation in macrophages in response to bacterial infection. We showed that mice with myeloid cell-specific deletion of *Mettl14* or with *Ythdf1* depletion suffered much higher mortality compared with control mice in both CLP- and LPS-induced sepsis models, due to the development of a severe and over-sustained cytokine storm. METTL14- or YTHDF1-deficient macrophages produced and maintained much higher levels of pro-inflammatory cytokines and chemokines in response to acute bacterial infection or LPS challenge because of impaired induction of SOCS1. We demonstrated that forced expression of SOCS1 in METTL14- or YTHDF1-deficient macrophages was able to correct their abnormalities, and reconstitution with these SOCS1-expressing mutant macrophages was able to rescue the severe septic phenotypes seen in mM14$^{-/-}$ and *Ythdf1*$^{-/-}$ mice. These observations provide compelling evidence that lack of sufficient SOCS1 induction in macrophages is the cause for the severe sepsis developed in these mutant mice.

We identified *Socs1* mRNA as a top target of m^{6}A methyltransferase in macrophage activation through unbiased global bioinformatic analyses. *Socs1* m^{6}A methylation is highly induced in macrophages following LPS stimulation, at least partly due to Zfp36-mediated *Fto* mRNA degradation. Zfp36 is the only ARE-binding protein that is induced by LPS in macrophages. Interestingly, Zfp36 has been suggested as a global post translational regulator of feedback control in inflammation (Tiedje, et al., 2016). FTO down-regulation helps sustain a high level of *Socs1* m^{6}A methylation, which allows sufficient and effective YTHDF1 binding to maintain *Socs1* mRNA stability and increase SOCS1 protein translation during macrophage septic response. YTHDF1 has been shown to control mRNA degradation and actively promote protein synthesis by interacting with the translation machinery (Wang, et al., 2015), and our data confirmed that m^{6}A-YTHDF1 interaction is required for new SOCS1 protein synthesis in macrophages following LPS challenge. The METTL14-YTHDF1-SOCS1 axis is a previously unknown mechanism to sustain an optimal level of SOCS1 in order to balance the inflammatory response during bacterial infection (Fig. 7I). Therefore, *Socs1* m^{6}A methylation provides another layer of SOCS1 regulation that is essential for a proper control of macrophage activation in TLR4-mediated inflammatory responses. Interestingly, METTL3, another subunit of m^{6}A methyltransferase, was recently shown to control naïve T cell homeostasis and differentiation by targeting a IL-7-STAT5-SOCS pathway via promoting *Socs1/3* mRNA degradation (Li, et al., 2017). An important implication from our study is that FTO might serve as a therapeutic target in anti-sepsis therapy, which is an attractive concept given that a number of small molecule FTO inhibitors have been developed for cancer treatment (Huang, et al., 2019; Chen, et al., 2012).

Cytokine storm represents a key feature of cytokine storm syndromes, a group of disorders representing a variety of inflammatory etiologies with a final common result of overwhelming systemic inflammation, hemodynamic instability, multi-organ dysfunction and potentially death (Canna and Behrens, 2012). Dysregulated macrophage activation has been implicated in these disorders (Crayne, et al., 2019; Karakike and Giamarellos-Bourboulis, 2019). In the COVID-19 pandemic caused by SARS-CoV-2 viral infection, COVID-19 patients in the ICU exhibited much higher serum pro-inflammatory cytokines compared to non-ICU patients, a sign of unresolved cytokine storm (Fu, et al., 2020). There is a belief that severe COVID-19 disease has features of cytokine storm syndromes and the

hyperinflammation needs to be suppressed to reduce mortality (Mahta, et al., 2020). SARS-CoV-2 coronavirus is believed to trigger cytokine storm through the TLR7/8-NF-κB signaling pathway (Felsenstein, et al., 2020). Therefore, how to control or suppress the cytokine storm is a significant question for many disorders with systemic inflammation. In this regard, our elucidation of a previously unknown regulatory mechanism in macrophage TLR4/NF-κB signaling has valuable therapeutic implications.

STAR Methods

RESOURCE AVAILABILITY

Lead contact—Further information and requests concerning resources and reagents should be directly addressed to Yan Chun Li (cyan@medicine.bsd.uchicago.edu).

Materials Availability—Lentiviruses, plasmid constructs and mouse lines generated in this study will be available from the corresponding author upon request.

Data and Code Availability—All datasets (RIP-seq and RNA-seq) generated in this study are available from GEO under the accession numbers GSE153511and GSE153512.

EXPEIMETAL MODEL AND SUBJECT DETAILS

Animals—*Mettl14*$^{flox/flox}$ mice carrying two LoxP sites flanking exons 7–9 in the *Mettl14* gene were initially produced in a 129/C57BL/6 mixed background by Chuan He's laboratory at the University of Chicago, and were then backcrossed to C57BL/6 background for 9 generations. *Ythdf1*$^{-/-}$ mice have been described previously (Shi, et al., 2018a). LysM-Cre transgenic mice (B6.129P2-*Lyz2*$^{tm1(cre)Ifo}$/J, Stock No. 004781) were purchased from Jackson Laboratory. *Mettl14*$^{flox/flox}$;LysM-Cre (mM14$^{-/-}$) mice were generated by crossing the two strains of mice. In all experiments 6 to 8-week old mice, both male and female, were used. All mice were housed at 25°C and maintained in a 12h/12hr light/dark cycle. All animal study protocols were approved by the Institutional Animal Care and Use Committee at the University of Chicago.

Cell lines—RAW264.7 mouse macrophage cell line (TIB-71) was purchased from ATCC. These cells were cultured in DMEM supplemented with 10% heat-inactivated fetal bovine serum (FBS), 100 U/ml penicillin and 100 μg/ml streptomycin at 37°C and 5% CO_2. L929 mouse fibroblast line (ATCC CCL-1) was cultured in DMEM supplemented with 10% heat-inactivated FBS, 100 U/ml penicillin and 100 μg/ml streptomycin at 37°C and 5% CO_2. L929 conditioned media were harvested 3 days after confluency, filtrated through 0.22 μm filters and stored at −80°C. HEK293T cells (ATCC CRL-3216) were cultured in DMEM supplemented with 10% FBS, 100 U/ml penicillin and 100 μg/ml streptomycin at 37°C and 5% CO_2.

Primary macrophage cultures—Peritoneal macrophages were harvested by injecting 5 ml PBS (pH 7.0) into the peritoneal cavity and collecting the peritoneal fluids after slowly rotating the mouse for 5 min. In some experiments, peritoneal macrophages were isolated following thioglycollate elicitation as described (Schneider, 2013). Peritoneal macrophages

were plated in RPMI1640 containing 10% heat-inactivated FBS, 100 U/ml penicillin and 100 μg/ml streptomycin, and unattached cells were removed after overnight culture at 37°C and 5% CO_2. Bone marrow derived macrophages (BMDMs) were obtained as described previously (Doyle, et al., 2002). Briefly, mouse bone marrow cells were flushed out of the femur and tibia with 10 ml RPMI using a syringe attached with a 26-G needle, and red blood cells were lysed with 10 mM NH_4Cl (pH8.0). The bone marrow cells were plated in RPMI1640 supplemented with 10% heat-inactivated FBS, 100 U/ml penicillin and 100 μg/ml streptomycin. After 5 hours of culture at 37°C and 5% CO_2 the unattached cells were collected and replated in RPMI1640 containing 10% FBS and 30% L929 conditioned media (Differentiation media). The cells were differentiated to BMDMs after 7 days. For lentiviral transduction, the unattached cells were incubated with a lentivirus at a MOI of 10 in RPMI1640 containing 10% FBS and 6 μg/ml polybrene for 48 hours before being cultured in the differentiation medium for 7 days. For LPS treatment, macrophages were incubated with LPS at 100 ng/ml for various times, and then cellular RNAs and/or cell lysates were prepared for analyses.

METHOD DETAILS

Lipopolysaccharide (LPS)-induced sepsis—Mice were administrated intraperitoneally with LPS (from E. Coli 0111:B4, L2630, Sigma-Aldrich) dissolved in PBS (pH7.0) at 20 mg/kg and then followed for up to 96 hours. Control mice were injected with 0.05 ml PBS. In some experiments, mice were killed at 24 hours after LPS injection. Mouse sera were collected through retra-orbital bleeding under anesthesia and stored at −80°C for later ELISA analysis of blood cytokines, and peritoneal macrophages were isolated and used for RNA preparation immediately.

Cecum ligation and puncture (CLP) procedure—CLP procedure was performed based on a published protocol (Tao, et al., 2005). In brief, mice were anesthetized with 2.5% isofluorane mixed with 100% oxygen. When the mice failed to respond to paw pinch, buprenophine was administered subcutaneously at 0.05 mg/kg prior to proper sterilization of the skin with 10% providone iodine, and then a midline abdominal incision was made. The cecum was exposed and ligated with a 3–0 silk tie 1 cm from the tip and the cecal wall perforated with a 20-gauge needle. The cecum was squeezed lightly to expose a small amount of stool to ensure complete perforation. Then the cecum was returned to the abdominal cavity, and the incision was closed. Immediately following the procedure, 0.5 ml of warmed normal saline was administered subcutaneously. Control mice underwent anesthesia, laparotomy and wound closure but not the cecal ligation and puncture procedures.

Lung histology—The lung was harvested immediately after mice were killed and fixed overnight in 4% formaldehyde made in PBS (pH 7.2) at room temperature. The tissue was then processed, embedded in paraffin wax and cut into 4 μm sections. The sections were stained by routine hematoxylin and eosin procedure.

Lung myeloperoxidase (MPO) activity—Lung lysate MPO activity was determined as detailed previously (Du, et al., 2015). Lung tissues were homogenized in 50 mM potassium

phosphate and 50 mM hexadecyl trimethyl ammonium bromide (HTAB), sonicated, snap frozen and thawed twice, followed by addition of 50 mM potassium phosphate containing 0.167 mg/ml O-dianisidine dihydrochloride and 0.0005% hydrogen peroxide. Absorbance was read at 460 nm using EL800 Universal Microplate Reader (Bio-Tek Instruments, Inc).

Cytokine quantification—Mouse TNF-α, IL-6, IL-1β and IFN-γ concentrations in the sera and in cell culture media were quantified using ELISA kits purchased from BioLegend (San Diego, CA) according to the manufacturer's instructions.

Lentiviral and plasmid constructs—Lentivirus that expresses METTL14, SOCS1 or FTO were constructed by cloning the coding region of human *METTL14* [NM_020961.4], *SOCS1* [NM_003745.1] or *FTO* [NM_001363894.1] cDNA into pLV[Exp]-Neo-EF1A lentiviral vector (VectorBuilder). All lentiviruses were produced with a titer of $>10^8$ pfu/ml. Expression plasmid pRP-mZfp36 was generated by cloning the coding region of mouse *Zfp36* cDNA into pRP-CMV vector (VectorBuilder). Luciferase (Luc) reporter plasmid pGL3-FTOARE was generated by cloning a 160 bp fragment from nucleotide (nt)3131 to 3291 at the 3'UTR of mouse *FTO* [NM_011936.2] cDNA to the downstream of Luc gene in pGL3-Promoter vector (Promega). This 160 bp fragment contains an AU-rich element (ARE) at nucleotide nt3148. pGL3-FTOAREmut was generated by mutating the nt3148 ARE sequence 5'UAUUUAAUU3' to 5'UAAAAAAUU3' mutant ARE sequence in pGL3-FTOARE plasmid using a QuickChange Site-Directed Mutagenesis Kit (Agilent). The mutation was confirmed by DNA sequencing.

Luciferase reporter assay—HEK293T cells were plated at 60–70% confluence onto 24-well plates and cultured in DMEM supplemented with 10% fetal bovine serum (FBS). After overnight culture, the cells were co-transfected with 500 ng pRP-mZfp36 or pRP-CMV and 500 ng pGL3-Promoter, pGL3-FTOARE or pGL3-FTOAREmut using Lipofectamine 3000 (Invitrogen). After 24 hrs, the cells were lysed and luciferease activity determined using a Bio-Glo Luciferase Assay System kit (Promega) in a Lumet LB 9507 luminometer (Berthold Technologies).

RT-PCR—Total RNAs were extracted using TRIzol reagent (ThermoFisher). First-strand cDNAs were synthesized using a ReverTra Ace qPCR RT kit (TOYOBO). Conventional PCR was carried out in a BioRad DNA Engine (BioRad). Real time PCR was carried out in a LightCycler 480 Instrument II real-time PCR system (Roche), using a SYBR Green Realtime PCR Master Mix kit (TOYOBO). The relative amounts of transcripts were calculated using the $2^{-\Delta\Delta Ct}$ formula (Schmittgen and Livak, 2008), normalized to GAPDH or beta-actin transcript as an internal control. PCR primers were listed in Table S1.

Western blotting—Tissue and cell samples were homogenized in Laemmli buffer. Protein concentration was determined using a Bio-Rad DC RC protein assay kit. Protein lysates were separated by SDS-PAGE and then electroblotted onto Immobilon-P membranes. The membranes were blotted with primary antibodies purchased commercially, followed by incubation with horseradish peroxidase-conjugated secondary antibody. Protein bands were visualized using chemiluminescence. Detailed Western blot procedures were described

previously (Li, et al., 2001). Primary antibodies used for Western blot analyses were listed in the Key Resources Table.

Bone marrow (BM) transplantation—BM transplantation was carried out based on previously published procedure (Szeto, et al., 2012). In brief, 6-week old recipient mice received lethal γ-irradiation of 1050 rads at 200 rads/min, and 6 hours later the mice were transplanted with donor BM cells at 5×10^6 BM cells/mouse (suspended in 0.1 ml PBS) through retra-orbital injection. Eight weeks after transplantation, the transplanted mice were used for LPS-induced sepsis models. To validate the success of BM transplantation, in parallel experiments CD45.1 recipient mice were lethally irradiated and transplanted with CD45.2 donor BM cells. Eight weeks after transplantation, FACS analysis confirmed that blood CD45.1 cells in the transplanted mice had been replaced by CD45.2 cells as shown previously (He, et al., 2019).

Macrophage depletion and reconstitution—Macrophages were depleted using clodronate-containing liposomes according to a published procedure (Weisser, et al., 2012). Mice were intravenously injected one dose of clodronate-liposomes (0.2 ml/mouse at 5 mg/ml, Encapsula NanoSciences). Elimination of $F4/80^+MHCII^+$ macrophages in the spleen was confirmed by FACS at 48 hrs. Two days after the clodronate-liposome treatment, macrophage-depleted mice were reconstituted with 2×10^6 fully differentiated BMDMs/mouse, dissolved in 0.2 ml PBS, through intravenous injection. In some experiments, the reconstituted BMDMs had been transduced with METTL14-lentivirus, SOCS1-lentivirus or FTO-lentivirus. Thirty-six hours after the reconstitution, these mice were challenged with PBS (pH7.0) or LPS (20 mg/kg) by intraperitoneal injection, and then closely monitored for up to 48 hours.

Flow cytometry—Spleens, harvested immediately after mice were killed, were smashed through 100 μm cell strainer to collect single cell suspension. Red blood cells were lysed by incubation with red blood cell lysis buffer at room temperature for 5 min. Cells were collected by centrifugation at 1500 rpm for 5 min for macrophage FACS analysis. Dead cells were excluded using a Live and Dead Violet Viability Kit (Invitrogen). Cell surface antigens were stained with anti-mouse MHCII FITC (clone M5/114.15.2), anti-mouse CD11b percp cy5.5 (clone M1/70) anti-mouse CD11c PE (clone N418) and anti-mouse F4/80 APC (clone BM8). All antibodies were purchased from BioLegend. Flow cytometric analysis was performed in a BD LSRFortessa unit (BD Biosciences) and data analyzed by FlowJo software V10.

m^6A quantitation—The amount of m^6A in total cellular RNAs was quantified using an EpiQuik m^6A RNA Methylation kit (Epigentek) according to manufacturer's instruction. The analysis of m^6A methylation was also performed by Northern blotting as described (Ausubel, et al., 1984). Briefly, total RNAs (20 μg/lane) were denatured in formaldehyde buffer, separated on a 1.2% agarose gel containing 2.2 M formaldehyde by electrophoresis and transferred onto a Nylon membrane (MSI, Westborough, MA). The membrane was incubated with anti-m^6A antibody at 4°C overnight, followed by incubation with horseradish

peroxidase-conjugated secondary antibody. The m^{6}A-containing RNAs were then visualized using chemiluminescence.

RNA-seq—Total RNAs were extracted from 3 sets of M14$^{f/f}$ and mM14$^{-/-}$ BMDMs treated with PBS or 100 ng/ml LPS for 6 hours, using TRIzol Reagent (ThermoFisher). Poly(A$^+$) mRNAs were subsequently purified from 3 μg total RNAs using a Dynabeads mRNA Purification Kit (ThermoFisher) and used for library construction. RNA-seq libraries were prepared using a SMARTer Stranded RNA-Seq Kit (TaKaRa) according to the manufacturer's instruction. The libraries were sequenced using an Illumina HiSeq 4000 System with single end 50-bp reads. Sequencing raw data were preprocessed using trim_galore v0.6.5, and reads were mapped by STAR (Dobin, et al., 2013) v2.6.1d against mm10 reference genome. Differential expression was analyzed using R and edgeR package. P-values were adjusted for multiple testing using the false discovery rate (FDR) correction of Benjamini and Hochberg (Benjamini and Hochberg, 1995). Significant genes were determined based on an FDR threshold of 5% (0.05). GO (Gene Ontology) biological process enrichment analysis of differentially expressed genes was accomplished using R and package clusterProfiler.

m^{6}A RIP-seq—Total RNAs were extracted from 3 sets of M14$^{f/f}$ and mM14$^{-/-}$ BMDMs treated with PBS or 100 ng/ml LPS for 6 hours, using TRIzol Reagent (ThermoFisher). Poly(A$^+$) mRNAs were purified from 20 μg total RNAs using a Dynabeads mRNA Purification Kit (ThermoFisher) and used for m6A RIP-seq. The poly(A$^+$) mRNAs were fragmented using RNA Fragmentation Reagents (ThermoFisher). A portion of fragmented mRNAs (4%) was saved as input control. The fragmented RNAs were incubated with anti-m6A antibody and m6A-IP was performed using an EpiMark N6-Methyladenosine Enrichment Kit (New England Biolabs) following the manufacturer's protocols. The IP-purified mRNA fragments were used to construct libraries using a SMARTer Stranded Total RNA-seq Kit v2-Pico Input Mammalian (TaKaRa). Sequencing of the libraries was carried out on an Illumina HiSeq 4000 Instrument with single-end 50-bp reads. Sequencing raw data were preprocessed by trim_galore v0.6.5 and then mapped against mm10 reference genome by HISAT2 (Kim, et al., 2015) v2.1.0. Peak calling was carried out using R package exomePeak (Meng, et al., 2013). Downstream analysis and visualization of data were accomplished using R v3.6. Motif search was performed using HOMER (Heinz, et al., 2010) v4.10.0. The longest isoform was retained if a gene has more than one isoforms.

m^{6}A RIP-qPCR—Poly(A$^+$) mRNAs were fragmented using RNA Fragmentation Reagents (ThermoFisher). A portion of fragmented mRNAs was saved as input control. Fragmented mRNAs were incubated with anti-m6A antibody, and antibody-bound mRNA fragments were purified using the EpiMark N6-Methyladenosine Enrichment Kit (New England Biolabs). The IP-purified mRNA fragments were reversed-transcribed into cDNA using hexamer random primer, and short sequences (100–150 bp) covering the m^{6}A sites were quantified by real time PCR. PCR primers are listed in Table S1. The enrichment of m^{6}A was determined by normalization to the input.

Cross-linking and RNA immunoprecipitation (CLIP) assay—CLIP assays were performed according to a previously described procedure (Bielli and Sette, 2017; Spitzer, et al., 2014; Hafner, et al., 2010) with some modifications. Briefly, cell cultures were treated with 4-thiouridine (100 μM) for 14 hours and LPS (100 ng/ml) for 6 hours. After washes with cold PBS (pH7.4), the cells were irradiated uncovered with UV light at 0.15 J/cm^2. The cells were collected in cold PBS by centrifugation. The pellets were re-dissolved in lysis buffer (50 mM HEPES-KOH (pH 7.5), 150 mM KCl, 2 mM EDTA-NaOH (PH 8.0), 1 mM NaF, 0.5% NP-40, 0.5 mM DTT, 1x protease inhibitor cocktail, 1 μl/ml RNase inhibitor) and incubated on ice for 10 min. The cell lysates were cleared by centrifugation at 13,000x g for 5 min and then filtered with a 0.2 μm filter, followed by 1 U/μl RNase T1 treatment at 22°C for 15 min. After saving 10% lysates for input, the rest of the lysates were mixed with antibody-conjugated protein G magnetic beads and rotated at cold room for 1 hour. The beads were collected with a magnet and washed 3× with an IP wash buffer (50 mM HEPES-KOH, 300 mM KCl, 0.05% NP-40, 0.5 mM DTT, 1x protease inhibitor cocktail). Then beads were treated with 100 U/μl RNase T1 at 22°C for 15 min, followed by 3× washes with a high-salt buffer (50 mM HEPES-KOH (pH 7.5), 500 mM KCl, 0.05% NP-40, 0.5 mM DTT, 0.5 μl/ml RNase inhibitor). The beads-RNA mixture was resuspended in a proteinase K buffer (100 mM Tris-HCl (pH 7.4), 150 mM NaCl, 12.5 mM EDTA, 2% SDS, 1.2 mg/ml proteinase K) and incubated at 55°C for 30 min. Input and co-immunoprecipitated RNAs were recovered by TRIzol Reagent extraction and co-precipitated with glycogen (10 μg/ml). The IP-purified RNA fragments were reversed transcribed into cDNA using random primers and quantified by real time PCR using primers listed in Table S1.

Assessment of mRNA decay—Macrophages cultured in 6-well plates were stimulated with LPS at 100 ng/ml for 6 hours, and then fresh media were added that contains actinomycin D at a final concentration of 5 μg/ml. Total cellular RNAs were extracted at 0, 2, 4, and 8 hours after actinomycin D treatment, and mRNA transcripts at each time point were quantified by real time RT-PCR. The mRNA level at each time point was normalized to that at 0 hour, and the changes were plotted against time.

Assessment of newly translated SOCS1 protein—Newly synthesized proteins in BMDMs were labelled with **L**-azidohomoalanine (AHA, Click Chemistry Tools). BMDMs were treated with PBS or LPS (100 ng/ml) for 6 hours (0 h label samples). At 3.5 and 4.5 hours into the treatment, the media were replaced with methionine (Met)-free RPMI1640. After 30 min starvation, the media were changed to Met-free RPMI1640 containing 40 μM AHA and incubation was continued for two hours (2 h label samples) and one hour (1 h label samples), respectively. At the end of 6 hours, the cells were washed with PBS and lysed with 1% SDS in 50 mM Tris–HCl (pH 8.0) containing protease inhibitors by sonication for 30 s. After incubation for 30 min on ice cell lysates were harvested after centrifugation at 12,000 × g for 20 min. Then 200 μg of lysates from each sample were subjected to biotinylation via Click reaction using Biotin-PGE4-Alkyne and a Click & Go Protein Reaction Buffer Kit (Click Chemistry Tools) according to the manufacture's instruction. The reaction was terminated by adding methanol and chloroform, and proteins were recovered according to a method described previously (Wessel and Flugge, 1984). The recovered protein pellets were air-dried and re-dissolved in RIPA buffer (50 mM Tris–HCl,

pH 7.5; 150 mM NaCl; 1% Triton X-100; 0.5% sodium deoxycholate; 0.1% SDS, 1% DTT, and protease inhibitors). After removing unsoluble materials by centrifugation (12,000 × g, 20 min), 1/10 material was saved as inputs, and then streptavidin-coated magnetic beads (High Capacity Streptavidin Magnetic Beads, Click Chemistry Tools) were added to precipitate the AHA-labelled proteins. After incubation for 2 hours at 4°C on a rotator, the beads were harvested on a magnetic stand. The beads were washed with 1% SDS made in PBS and proteins were dissolved in Laemmli buffer. After boiling, the proteins were separated by SDS-PAGE, and the nascent SOCS1 protein was visualized by Western blotting. The inputs were also used for Western blotting to measure total SOCS1 and β-actin.

QUANTIFICATION AND STATISTICAL ANALYSIS

Data values were presented as means ± SD. Most experiments were repeated at least twice. All bioinformatic analyses were conducted using samples of biological triplicates. Statistical analyses were performed using GraphPad Prism Version 8.4.2. For two group comparisons unpaired two-tailed Student's *t*-test was used, and for three or more group comparisons ordinary one-way or two-way analysis of variance (ANOVA) was performed. Animal survival rates were estimated by the Kaplan-Meier method and groups were analyzed by the log-rank test. Comparisons between cumulative fraction were performed by Mann-Whitney test. P values < 0.05 were considered statistically significant.

Supplementary Material

Refer to Web version on PubMed Central for supplementary material.

Acknowledgements

This work was supported in part by National Institutes of Health grants R21AI140152 (Y.C.L), R01AI151162 (Y.C.L), RM1HG008935 (C.H.) and 5UL1TR002389. C.H. is an Howard Hughes Medical Institute Investigator. We thank Youyang Zhao (Northwestern University) for technical advices for the CLP procedure.

REFERENCES

Alarcon CR, Goodarzi H, Lee H, Liu X, Tavazoie S, and Tavazoie SF (2015). HNRNPA2B1 Is a Mediator of m(6)A-Dependent Nuclear RNA Processing Events. Cell 162, 1299–308. [PubMed: 26321680]

Angus DC, and van der Poll T. (2013). Severe sepsis and septic shock. N Engl J Med 369, 840–51. [PubMed: 23984731]

Ausubel FM, Brent R, Kinston RE, Moore DD, Seidman JG, Smith JA, and Struhl K. (1984). Current protocols in molecular biology (New York: John Wiley & Sons)

Baetz A, Frey M, Heeg K, and Dalpke AH (2004). Suppressor of cytokine signaling (SOCS) proteins indirectly regulate toll-like receptor signaling in innate immune cells. J Biol Chem 279, 54708–15. [PubMed: 15491991]

Batista PJ, Molinie B, Wang J, Qu K, Zhang J, Li L, Bouley DM, Lujan E, Haddad B, Daneshvar K, et al. (2014). m(6)A RNA modification controls cell fate transition in mammalian embryonic stem cells. Cell Stem Cell 15, 707–19. [PubMed: 25456834]

Benjamini Y, and Hochberg Y. (1995). Controlling the False Discovery Rate - a Practical and Powerful Approach to Multiple Testing. J R Stat Soc B 57, 289–300.

Beutler B. (2004). Inferences, questions and possibilities in Toll-like receptor signalling. Nature 430, 257–63. [PubMed: 15241424]

Bielli P, and Sette C. (2017). Analysis of in vivo Interaction between RNA Binding Proteins and Their RNA Targets by UV Cross-linking and Immunoprecipitation (CLIP) Method. Bio Protoc 7.

Bolognani F, and Perrone-Bizzozero NI (2008). RNA-protein interactions and control of mRNA stability in neurons. J Neurosci Res 86, 481–9. [PubMed: 17853436]

Boone DL, Turer EE, Lee EG, Ahmad RC, Wheeler MT, Tsui C, Hurley P, Chien M, Chai S, Hitotsumatsu O, et al. (2004). The ubiquitin-modifying enzyme A20 is required for termination of Toll-like receptor responses. Nat Immunol 5, 1052–60. [PubMed: 15334086]

Brint EK, Xu D, Liu H, Dunne A, McKenzie AN, O'Neill LA, and Liew FY (2004). ST2 is an inhibitor of interleukin 1 receptor and Toll-like receptor 4 signaling and maintains endotoxin tolerance. Nat Immunol 5, 373–9. [PubMed: 15004556]

Canna SW, and Behrens EM (2012). Making sense of the cytokine storm: a conceptual framework for understanding, diagnosing, and treating hemophagocytic syndromes. Pediatr Clin North Am 59, 329–44. [PubMed: 22560573]

Chaudhry H, Zhou J, Zhong Y, Ali MM, McGuire F, Nagarkatti PS, and Nagarkatti M. (2013). Role of cytokines as a double-edged sword in sepsis. In Vivo 27, 669–84. [PubMed: 24292568]

Chen B, Ye F, Yu L, Jia G, Huang X, Zhang X, Peng S, Chen K, Wang M, Gong S, et al. (2012). Development of cell-active N6-methyladenosine RNA demethylase FTO inhibitor. J Am Chem Soc 134, 17963–71. [PubMed: 23045983]

Chen T, Hao YJ, Zhang Y, Li MM, Wang M, Han W, Wu Y, Lv Y, Hao J, Wang L, et al. (2015). m(6)A RNA methylation is regulated by microRNAs and promotes reprogramming to pluripotency. Cell Stem Cell 16, 289–301. [PubMed: 25683224]

Chen Y, Liu W, Sun T, Huang Y, Wang Y, Deb DK, Yoon D, Kong J, Thadhani R, and Li YC (2013). 1,25-Dihydroxyvitamin D Promotes Negative Feedback Regulation of TLR Signaling via Targeting MicroRNA-155-SOCS1 in Macrophages. J Immunol 190, 3687–95. [PubMed: 23436936]

Clausen BE, Burkhardt C, Reith W, Renkawitz R, and Forster I. (1999). Conditional gene targeting in macrophages and granulocytes using LysMcre mice. Transgenic Res 8, 265–77. [PubMed: 10621974]

Coperchini F, Chiovato L, Croce L, Magri F, and Rotondi M. (2020). The cytokine storm in COVID-19: An overview of the involvement of the chemokine/chemokine-receptor system. Cytokine Growth Factor Rev.

Crayne CB, Albeituni S, Nichols KE, and Cron RQ (2019). The Immunology of Macrophage Activation Syndrome. Front Immunol 10, 119. [PubMed: 30774631]

Cui Q, Shi H, Ye P, Li L, Qu Q, Sun G, Sun G, Lu Z, Huang Y, Yang CG, et al. (2017). m6A RNA Methylation Regulates the Self-Renewal and Tumorigenesis of Glioblastoma Stem Cells. Cell Rep 18, 2622–2634. [PubMed: 28297667]

Dejager L, Pinheiro I, Dejonckheere E, and Libert C. (2011). Cecal ligation and puncture: the gold standard model for polymicrobial sepsis? Trends Microbiol 19, 198–208. [PubMed: 21296575]

Dobin A, Davis CA, Schlesinger F, Drenkow J, Zaleski C, Jha S, Batut P, Chaisson M, and Gingeras TR (2013). STAR: ultrafast universal RNA-seq aligner. Bioinformatics 29, 15–21. [PubMed: 23104886]

Dominissini D, Moshitch-Moshkovitz S, Salmon-Divon M, Amariglio N, and Rechavi G. (2013). Transcriptome-wide mapping of N(6)-methyladenosine by m(6)A-seq based on immunocapturing and massively parallel sequencing. Nat Protoc 8, 176–89. [PubMed: 23288318]

Dominissini D, Moshitch-Moshkovitz S, Schwartz S, Salmon-Divon M, Ungar L, Osenberg S, Cesarkas K, Jacob-Hirsch J, Amariglio N, Kupiec M, et al. (2012). Topology of the human and mouse m6A RNA methylomes revealed by m6A-seq. Nature 485, 201–6. [PubMed: 22575960]

Doyle S, Vaidya S, O'Connell R, Dadgostar H, Dempsey P, Wu T, Rao G, Sun R, Haberland M, Modlin R, et al. (2002). IRF3 mediates a TLR3/TLR4-specific antiviral gene program. Immunity 17, 251–63. [PubMed: 12354379]

Du H, Zhao Y, He J, Zhang Y, Xi H, Liu M, Ma J, and Wu L. (2016). YTHDF2 destabilizes m(6)A-containing RNA through direct recruitment of the CCR4-NOT deadenylase complex. Nat Commun 7, 12626. [PubMed: 27558897]

Du J, Chen Y, Shi Y, Liu T, Cao Y, Tang Y, Ge X, Nie H, Zheng C, and Li YC (2015). 1,25-Dihydroxyvitamin D Protects Intestinal Epithelial Barrier by Regulating the Myosin Light Chain Kinase Signaling Pathway. Inflamm Bowel Dis 21, 2495–506. [PubMed: 26287999]

Duncan SA, Baganizi DR, Sahu R, Singh SR, and Dennis VA (2017). SOCS Proteins as Regulators of Inflammatory Responses Induced by Bacterial Infections: A Review. Front Microbiol 8, 2431. [PubMed: 29312162]

Endo TA, Masuhara M, Yokouchi M, Suzuki R, Sakamoto H, Mitsui K, Matsumoto A, Tanimura S, Ohtsubo M, Misawa H, et al. (1997). A new protein containing an SH2 domain that inhibits JAK kinases. Nature 387, 921–4. [PubMed: 9202126]

Felsenstein S, Herbert JA, McNamara PS, and Hedrich CM (2020). COVID-19: Immunology and treatment options. Clin Immunol 215, 108448.

Fortier ME, Kent S, Ashdown H, Poole S, Boksa P, and Luheshi GN (2004). The viral mimic, polyinosinic:polycytidylic acid, induces fever in rats via an interleukin-1-dependent mechanism. Am J Physiol Regul Integr Comp Physiol 287, R759–66. [PubMed: 15205185]

Fu Y, Cheng Y, and Wu Y. (2020). Understanding SARS-CoV-2-Mediated Inflammatory Responses: From Mechanisms to Potential Therapeutic Tools. Virol Sin.

Geula S, Moshitch-Moshkovitz S, Dominissini D, Mansour AA, Kol N, Salmon-Divon M, Hershkovitz V, Peer E, Mor N, Manor YS, et al. (2015). Stem cells. m6A mRNA methylation facilitates resolution of naive pluripotency toward differentiation. Science 347, 1002–6. [PubMed: 25569111]

Gordon S, and Martinez FO (2010). Alternative activation of macrophages: mechanism and functions. Immunity 32, 593–604. [PubMed: 20510870]

Guhaniyogi J, and Brewer G. (2001). Regulation of mRNA stability in mammalian cells. Gene 265, 11–23. [PubMed: 11255003]

Hafner M, Landthaler M, Burger L, Khorshid M, Hausser J, Berninger P, Rothballer A, Ascano M, Jungkamp AC, Munschauer M, et al. (2010). PAR-CliP--a method to identify transcriptome-wide the binding sites of RNA binding proteins. J Vis Exp.

He L, Zhou M, and Li YC (2019). Vitamin D/Vitamin D Receptor Signaling Is Required for Normal Development and Function of Group 3 Innate Lymphoid Cells in the Gut. iScience 17, 119–131. [PubMed: 31272068]

Heinz S, Benner C, Spann N, Bertolino E, Lin YC, Laslo P, Cheng JX, Murre C, Singh H, and Glass CK (2010). Simple combinations of lineage-determining transcription factors prime cis-regulatory elements required for macrophage and B cell identities. Mol Cell 38, 576–89. [PubMed: 20513432]

Huang H, Weng H, Sun W, Qin X, Shi H, Wu H, Zhao BS, Mesquita A, Liu C, Yuan CL, et al. (2018). Recognition of RNA N(6)-methyladenosine by IGF2BP proteins enhances mRNA stability and translation. Nat Cell Biol 20, 285–295. [PubMed: 29476152]

Huang Y, Su R, Sheng Y, Dong L, Dong Z, Xu H, Ni T, Zhang ZS, Zhang T, Li C, et al. (2019). Small-Molecule Targeting of Oncogenic FTO Demethylase in Acute Myeloid Leukemia. Cancer Cell 35, 677–691 e10. [PubMed: 30991027]

Janssens S, Burns K, Tschopp J, and Beyaert R. (2002). Regulation of interleukin-1- and lipopolysaccharide-induced NF-kappaB activation by alternative splicing of MyD88. Curr Biol 12, 467–71. [PubMed: 11909531]

Kagan JC, and Medzhitov R. (2006). Phosphoinositide-mediated adaptor recruitment controls Toll-like receptor signaling. Cell 125, 943–55. [PubMed: 16751103]

Kane SE, and Beemon K. (1985). Precise localization of m6A in Rous sarcoma virus RNA reveals clustering of methylation sites: implications for RNA processing. Mol Cell Biol 5, 2298–306. [PubMed: 3016525]

Karakike E, and Giamarellos-Bourboulis EJ (2019). Macrophage Activation-Like Syndrome: A Distinct Entity Leading to Early Death in Sepsis. Front Immunol 10, 55. [PubMed: 30766533]

Kawai T, and Akira S. (2007). Signaling to NF-kappaB by Toll-like receptors. Trends Mol Med 13, 460–9. [PubMed: 18029230]

Kim D, Langmead B, and Salzberg SL (2015). HISAT: a fast spliced aligner with low memory requirements. Nat Methods 12, 357–60. [PubMed: 25751142]

Kimura A, Naka T, Muta T, Takeuchi O, Akira S, Kawase I, and Kishimoto T. (2005). Suppressor of cytokine signaling-1 selectively inhibits LPS-induced IL-6 production by regulating JAK-STAT. Proceedings of the National Academy of Sciences of the United States of America 102, 17089–94. [PubMed: 16287972]

Kinjyo I, Hanada T, Inagaki-Ohara K, Mori H, Aki D, Ohishi M, Yoshida H, Kubo M, and Yoshimura A. (2002). SOCS1/JAB is a negative regulator of LPS-induced macrophage activation. Immunity 17, 583–91. [PubMed: 12433365]

Kobayashi K, Hernandez LD, Galan JE, Janeway CA Jr., Medzhitov R, and Flavell RA (2002). IRAK-M is a negative regulator of Toll-like receptor signaling. Cell 110, 191–202. [PubMed: 12150927]

Koranda JL, Dore L, Shi H, Patel MJ, Vaasjo LO, Rao MN, Chen K, Lu Z, Yi Y, Chi W, et al. (2018). Mettl14 Is Essential for Epitranscriptomic Regulation of Striatal Function and Learning. Neuron 99, 283–292 e5. [PubMed: 30056831]

Krebs DL, and Hilton DJ (2000). SOCS: physiological suppressors of cytokine signaling. J Cell Sci 113 (Pt 16), 2813–9. [PubMed: 10910765]

Lee H, Bao S, Qian Y, Geula S, Leslie J, Zhang C, Hanna JH, and Ding L. (2019). Stage-specific requirement for Mettl3-dependent m(6)A mRNA methylation during haematopoietic stem cell differentiation. Nat Cell Biol.

Li HB, Tong J, Zhu S, Batista PJ, Duffy EE, Zhao J, Bailis W, Cao G, Kroehling L, Chen Y, et al. (2017). m6A mRNA methylation controls T cell homeostasis by targeting the IL-7/STAT5/SOCS pathways. Nature 548, 338–342. [PubMed: 28792938]

Li YC, Bolt MJG, Cao L-P, and Sitrin MD (2001). Effects of vitamin D receptor inactivation on the expression of calbindins and calcium metabolism. Am J Physiol Endocrinol Metab 281, E558–E564. [PubMed: 11500311]

Liew FY, Xu D, Brint EK, and O'Neill LA (2005). Negative regulation of toll-like receptor-mediated immune responses. Nat Rev Immunol 5, 446–58. [PubMed: 15928677]

Liu J, Dou X, Chen C, Chen C, Liu C, Xu MM, Zhao S, Shen B, Gao Y, Han D, et al. (2020). N (6)-methyladenosine of chromosome-associated regulatory RNA regulates chromatin state and transcription. Science 367, 580–586. [PubMed: 31949099]

Lu LF, Gasteiger G, Yu IS, Chaudhry A, Hsin JP, Lu Y, Bos PD, Lin LL, Zawislak CL, Cho S, et al. (2015). A Single miRNA-mRNA Interaction Affects the Immune Response in a Context- and Cell-Type-Specific Manner. Immunity 43, 52–64. [PubMed: 26163372]

Mahta P, McAuley DF, Brown M, Sanchez E, Tattershal RS, and Manson JJ (2020). COVID-19: consider cytokine storm syndromes and immunosuppression. Lancet 395, 1033. [PubMed: 32192578]

Mansell A, Brint E, Gould JA, O'Neill LA, and Hertzog PJ (2004). Mal interacts with tumor necrosis factor receptor-associated factor (TRAF)-6 to mediate NF-kappaB activation by toll-like receptor (TLR)-2 and TLR4. J Biol Chem 279, 37227–30. [PubMed: 15247281]

Mansell A, Smith R, Doyle SL, Gray P, Fenner JE, Crack PJ, Nicholson SE, Hilton DJ, O'Neill LA, and Hertzog PJ (2006). Suppressor of cytokine signaling 1 negatively regulates Toll-like receptor signaling by mediating Mal degradation. Nat Immunol 7, 148–55. [PubMed: 16415872]

Marine JC, Topham DJ, McKay C, Wang D, Parganas E, Stravopodis D, Yoshimura A, and Ihle JN (1999). SOCS1 deficiency causes a lymphocyte-dependent perinatal lethality. Cell 98, 609–16. [PubMed: 10490100]

Meng J, Cui X, Rao MK, Chen Y, and Huang Y. (2013). Exome-based analysis for RNA epigenome sequencing data. Bioinformatics 29, 1565–7. [PubMed: 23589649]

Mortazavi A, Williams BA, McCue K, Schaeffer L, and Wold B. (2008). Mapping and quantifying mammalian transcriptomes by RNA-Seq. Nat Methods 5, 621–8. [PubMed: 18516045]

Nachtergaele S, and He C. (2017). The emerging biology of RNA post-transcriptional modifications. RNA Biol 14, 156–163. [PubMed: 27937535]

Naito M, Nagai H, Kawano S, Umezu H, Zhu H, Moriyama H, Yamamoto T, Takatsuka H, and Takei Y. (1996). Liposome-encapsulated dichloromethylene diphosphonate induces macrophage apoptosis in vivo and in vitro. J Leukoc Biol 60, 337–44. [PubMed: 8830790]

Naka T, Narazaki M, Hirata M, Matsumoto T, Minamoto S, Aono A, Nishimoto N, Kajita T, Taga T, Yoshizaki K, et al. (1997). Structure and function of a new STAT-induced STAT inhibitor. Nature 387, 924–9. [PubMed: 9202127]

Nakagawa R, Naka T, Tsutsui H, Fujimoto M, Kimura A, Abe T, Seki E, Sato S, Takeuchi O, Takeda K, et al. (2002). SOCS-1 participates in negative regulation of LPS responses. Immunity 17, 677–87. [PubMed: 12433373]

Narayan P, and Rottman FM (1988). An in vitro system for accurate methylation of internal adenosine residues in messenger RNA. Science 242, 1159–62. [PubMed: 3187541]

O'Connell RM, Taganov KD, Boldin MP, Cheng G, and Baltimore D. (2007). MicroRNA-155 is induced during the macrophage inflammatory response. Proceedings of the National Academy of Sciences of the United States of America 104, 1604–9. [PubMed: 17242365]

Raetz CR, and Whitfield C. (2002). Lipopolysaccharide endotoxins. Annu Rev Biochem 71, 635–700. [PubMed: 12045108]

Rhee C, Dantes R, Epstein L, Murphy DJ, Seymour CW, Iwashyna TJ, Kadri SS, Angus DC, Danner RL, Fiore AE, et al. (2017). Incidence and Trends of Sepsis in US Hospitals Using Clinical vs Claims Data, 2009–2014. JAMA 318, 1241–1249. [PubMed: 28903154]

Ruggiero T, Trabucchi M, De Santa F, Zupo S, Harfe BD, McManus MT, Rosenfeld MG, Briata P, and Gherzi R. (2009). LPS induces KH-type splicing regulatory protein-dependent processing of microRNA-155 precursors in macrophages. Faseb J 23, 2898–908. [PubMed: 19423639]

Ryo A, Suizu F, Yoshida Y, Perrem K, Liou YC, Wulf G, Rottapel R, Yamaoka S, and Lu KP (2003). Regulation of NF-kappaB signaling by Pin1-dependent prolyl isomerization and ubiquitinmediated proteolysis of p65/RelA. Mol Cell 12, 1413–26. [PubMed: 14690596]

Schmittgen TD, and Livak KJ (2008). Analyzing real-time PCR data by the comparative C(T) method. Nat Protoc 3, 1101–8. [PubMed: 18546601]

Schneider M. (2013). Collecting resident or thioglycollate-elicited peritoneal macrophages. Methods Mol Biol 1031, 37–40. [PubMed: 23824884]

Shaw G, and Kamen R. (1986). A conserved AU sequence from the 3' untranslated region of GM-CSF mRNA mediates selective mRNA degradation. Cell 46, 659–67. [PubMed: 3488815]

Shi H, Wang X, Lu Z, Zhao BS, Ma H, Hsu PJ, Liu C, and He C. (2017). YTHDF3 facilitates translation and decay of N6-methyladenosine-modified RNA. Cell Res 27, 315–328. [PubMed: 28106072]

Shi H, Zhang X, Weng YL, Lu Z, Liu Y, Lu Z, Li J, Hao P, Zhang Y, Zhang F, et al. (2018a). m(6)A facilitates hippocampus-dependent learning and memory through YTHDF1. Nature 563, 249–253. [PubMed: 30401835]

Shi J, Hua L, Harmer D, Li P, and Ren G. (2018b). Cre Driver Mice Targeting Macrophages. Methods Mol Biol 1784, 263–275. [PubMed: 29761406]

Spitzer J, Hafner M, Landthaler M, Ascano M, Farazi T, Wardle G, Nusbaum J, Khorshid M, Burger L, Zavolan M, et al. (2014). PAR-CLIP (Photoactivatable Ribonucleoside-Enhanced Crosslinking and Immunoprecipitation): a step-by-step protocol to the transcriptome-wide identification of binding sites of RNA-binding proteins. Methods Enzymol 539, 113–61. [PubMed: 24581442]

Starr R, Willson TA, Viney EM, Murray LJ, Rayner JR, Jenkins BJ, Gonda TJ, Alexander WS, Metcalf D, Nicola NA, et al. (1997). A family of cytokine-inducible inhibitors of signalling. Nature 387, 917–21. [PubMed: 9202125]

Strebovsky J, Walker P, Lang R, and Dalpke AH (2011). Suppressor of cytokine signaling 1 (SOCS1) limits NFkappaB signaling by decreasing p65 stability within the cell nucleus. FASEB J 25, 863–74. [PubMed: 21084693]

Szeto FL, Reardon CA, Yoon D, Wang Y, Wong KE, Chen Y, Kong J, Liu SQ, Thadhani R, Getz GS, et al. (2012). Vitamin D receptor signaling inhibits atherosclerosis in mice. Mol Endocrinol 26, 1091–101. [PubMed: 22638071]

Tao W, Enoh VT, Lin CY, Johnston WE, Li P, and Sherwood ER (2005). Cardiovascular dysfunction caused by cecal ligation and puncture is attenuated in CD8 knockout mice treated with anti-asialoGM1. Am J Physiol Regul Integr Comp Physiol 289, R478–R485. [PubMed: 15845883]

Tiedje C, Diaz-Munoz MD, Trulley P, Ahlfors H, Laass K, Blackshear PJ, Turner M, and Gaestel M. (2016). The RNA-binding protein TTP is a global post-transcriptional regulator of feedback control in inflammation. Nucleic Acids Res 44, 7418–40. [PubMed: 27220464]

Tiedje C, Kotlyarov A, and Gaestel M. (2010). Molecular mechanisms of phosphorylation-regulated TTP (tristetraprolin) action and screening for further TTP-interacting proteins. Biochem Soc Trans 38, 1632–7. [PubMed: 21118139]

Toscano MG, Ganea D, and Gamero AM (2011). Cecal ligation puncture procedure. J Vis Exp.

van der Poll T, van de Veerdonk FL, Scicluna BP, and Netea MG (2017). The immunopathology of sepsis and potential therapeutic targets. Nat Rev Immunol 17, 407–420. [PubMed: 28436424]

van Rooijen N, Sanders A, and van den Berg TK (1996). Apoptosis of macrophages induced by liposome-mediated intracellular delivery of clodronate and propamidine. J Immunol Methods 193, 93–9. [PubMed: 8690935]

Verstak B, Nagpal K, Bottomley SP, Golenbock DT, Hertzog PJ, and Mansell A. (2009). MyD88 adapter-like (Mal)/TIRAP interaction with TRAF6 is critical for TLR2- and TLR4-mediated NF-kappaB proinflammatory responses. J Biol Chem 284, 24192–203. [PubMed: 19592497]

Vincent JL, Rello J, Marshall J, Silva E, Anzueto A, Martin CD, Moreno R, Lipman J, Gomersall C, Sakr Y, et al. (2009). International study of the prevalence and outcomes of infection in intensive care units. JAMA 302, 2323–9. [PubMed: 19952319]

Wang P, Hou J, Lin L, Wang C, Liu X, Li D, Ma F, Wang Z, and Cao X. (2010). Inducible microRNA-155 feedback promotes type I IFN signaling in antiviral innate immunity by targeting suppressor of cytokine signaling 1. J Immunol 185, 6226–33. [PubMed: 20937844]

Wang X, Lu Z, Gomez A, Hon GC, Yue Y, Han D, Fu Y, Parisien M, Dai Q, Jia G, et al. (2014a). N6-methyladenosine-dependent regulation of messenger RNA stability. Nature 505, 117–20. [PubMed: 24284625]

Wang X, Zhao BS, Roundtree IA, Lu Z, Han D, Ma H, Weng X, Chen K, Shi H, and He C. (2015). N(6)-methyladenosine Modulates Messenger RNA Translation Efficiency. Cell 161, 1388–99. [PubMed: 26046440]

Wang Y, Li Y, Toth JI, Petroski MD, Zhang Z, and Zhao JC (2014b). N6-methyladenosine modification destabilizes developmental regulators in embryonic stem cells. Nat Cell Biol 16, 191–8. [PubMed: 24394384]

Wei CM, Gershowitz A, and Moss B. (1975). Methylated nucleotides block 5' terminus of HeLa cell messenger RNA. Cell 4, 379–86. [PubMed: 164293]

Weisser SB, van Rooijen N, and Sly LM (2012). Depletion and reconstitution of macrophages in mice. J Vis Exp, 4105.

Weng H, Huang H, Wu H, Qin X, Zhao BS, Dong L, Shi H, Skibbe J, Shen C, Hu C, et al. (2018). METTL14 Inhibits Hematopoietic Stem/Progenitor Differentiation and Promotes Leukemogenesis via mRNA m(6)A Modification. Cell Stem Cell 22, 191–205 e9. [PubMed: 29290617]

Wessel D, and Flugge UI (1984). A method for the quantitative recovery of protein in dilute solution in the presence of detergents and lipids. Anal Biochem 138, 141–3. [PubMed: 6731838]

Winstall E, Gamache M, and Raymond V. (1995). Rapid mRNA degradation mediated by the c-fos 3' AU-rich element and that mediated by the granulocyte-macrophage colony-stimulating factor 3' AU-rich element occur through similar polysome-associated mechanisms. Mol Cell Biol 15, 3796–804. [PubMed: 7540719]

Yoshimura A, Naka T, and Kubo M. (2007). SOCS proteins, cytokine signalling and immune regulation. Nat Rev Immunol 7, 454–65. [PubMed: 17525754]

Zhang S, Zhao BS, Zhou A, Lin K, Zheng S, Lu Z, Chen Y, Sulman EP, Xie K, Bogler O, et al. (2017). m6A Demethylase ALKBH5 Maintains Tumorigenicity of Glioblastoma Stem-like Cells by Sustaining FOXM1 Expression and Cell Proliferation Program. Cancer Cell 31, 591–606 e6. [PubMed: 28344040]

Zhao BS, Roundtree IA, and He C. (2017). Post-transcriptional gene regulation by mRNA modifications. Nat Rev Mol Cell Biol 18, 31–42. [PubMed: 27808276]

Zhou J, Wan J, Gao X, Zhang X, Jaffrey SR, and Qian SB (2015a). Dynamic m(6)A mRNA methylation directs translational control of heat shock response. Nature 526, 591–4. [PubMed: 26458103]

Zhou X, Liu Z, Cheng X, Zheng Y, Zeng F, and He Y. (2015b). Socs1 and Socs3 degrades Traf6 via polyubiquitination in LPS-induced acute necrotizing pancreatitis. Cell Death Dis 6, e2012.

Highlights

- Macrophages depleted of m^{6}A methylation are overactivated upon bacterial infection
- m^{6}A methylation is required to maintain SOCS1 induction to control cytokine storm
- METTL14-m^{6}A-YTHDF1 axis up-regulates SOCS1 in macrophage response to infection
- Zfp36/ARE-mediated *Fto* mRNA degradation promotes *Socs1* m^{6}A methylation

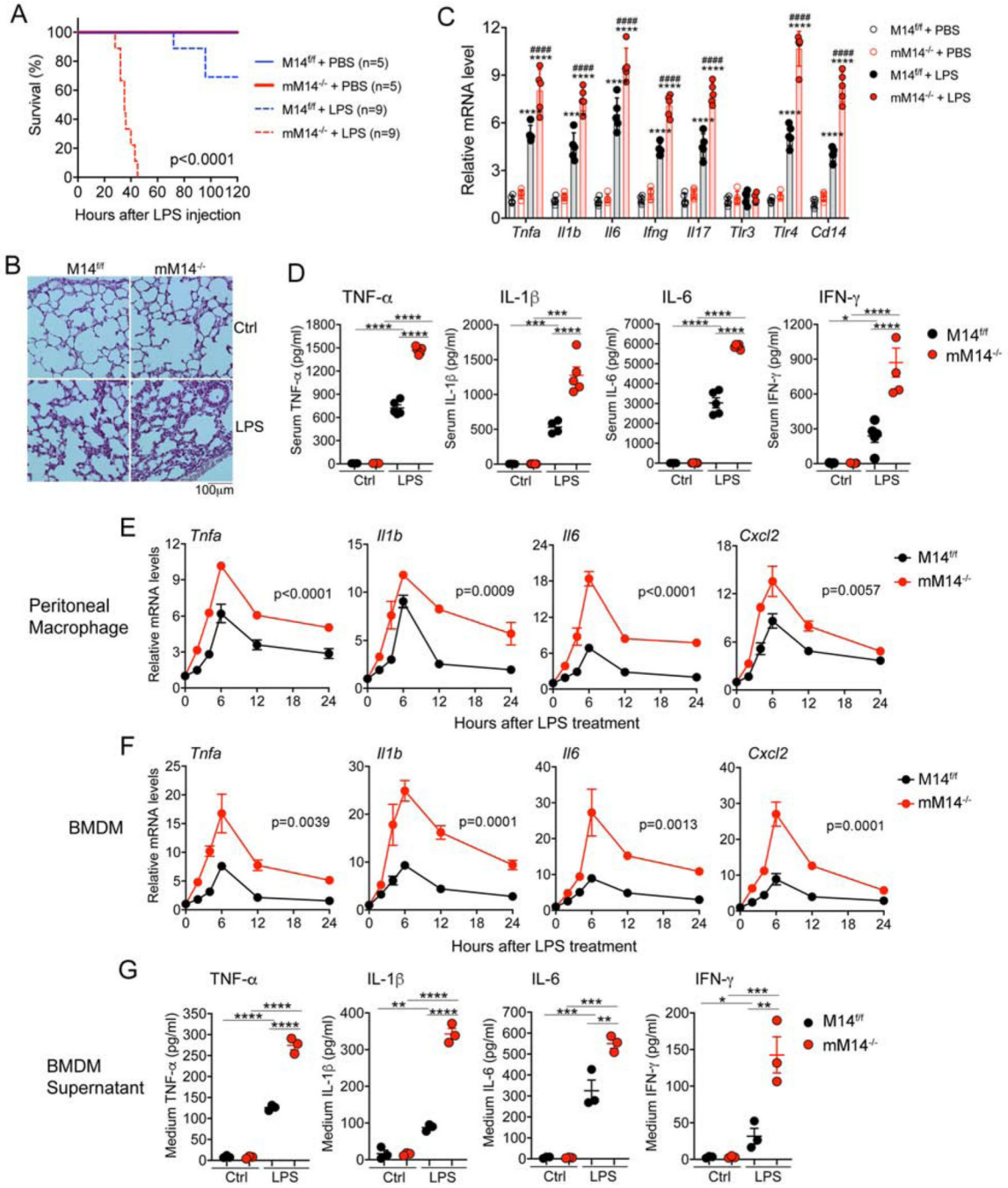

Figure 1. Mice with myeloid cell-specific deletion of METTL14 are hyper responsive to LPS challenge.

(A) Kaplan-Meier survival curves of $M14^{f/f}$ and $mM14^{-/-}$ mice following LPS or PBS (Ctrl) treatment, n=5 or 9 each group; p<0.0001, $mM14^{-/-}$ + LPS vs. $M14^{f/f}$ + LPS;

(B) Lung histology of $M14^{f/f}$ and $mM14^{-/-}$ mice by H&E staining at 24 hr post LPS challenge;

(C) RT-qPCR quantitation of transcripts of pro-inflammatory cytokines, TLR3, TLR4 and CD14 in peritoneal macrophages freshly isolated from $M14^{f/f}$ and $mM14^{-/-}$ mice at 6 hr

after LPS challenge; n=5 each group; ****P<0.0001 vs. corresponding PBS; ####P<0.0001 vs. corresponding LPS, by one-way ANOVA Tukey multiple comparison test;
(D) Serum pro-inflammatory cytokine concentrations in $M14^{f/f}$ and $mM14^{-/-}$ mice at 24 hr after LPS challenge, n=5 each group;
(E) Time course expression of pro-inflammatory cytokine transcripts in cultured $M14^{f/f}$ and $mM14^{-/-}$ peritoneal macrophages following LPS stimulation, n=3 each group;
(F) Time course expression of pro-inflammatory cytokine transcripts in cultured $M14^{f/f}$ and $mM14^{-/-}$ BMDMs following LPS stimulation, n=3 each group;
(G) Pro-inflammatory cytokine concentrations in the supernatants of cultured $M14^{f/f}$ and $mM14^{-/-}$ BMDMs treated with LPS for 24 hrs, n=3 each group; *P<0.05, **P<0.01; ***P<0.001; ****P<0.0001 by two-way ANOVA Tukey multiple comparison test. Data are presented as mean ± SD.

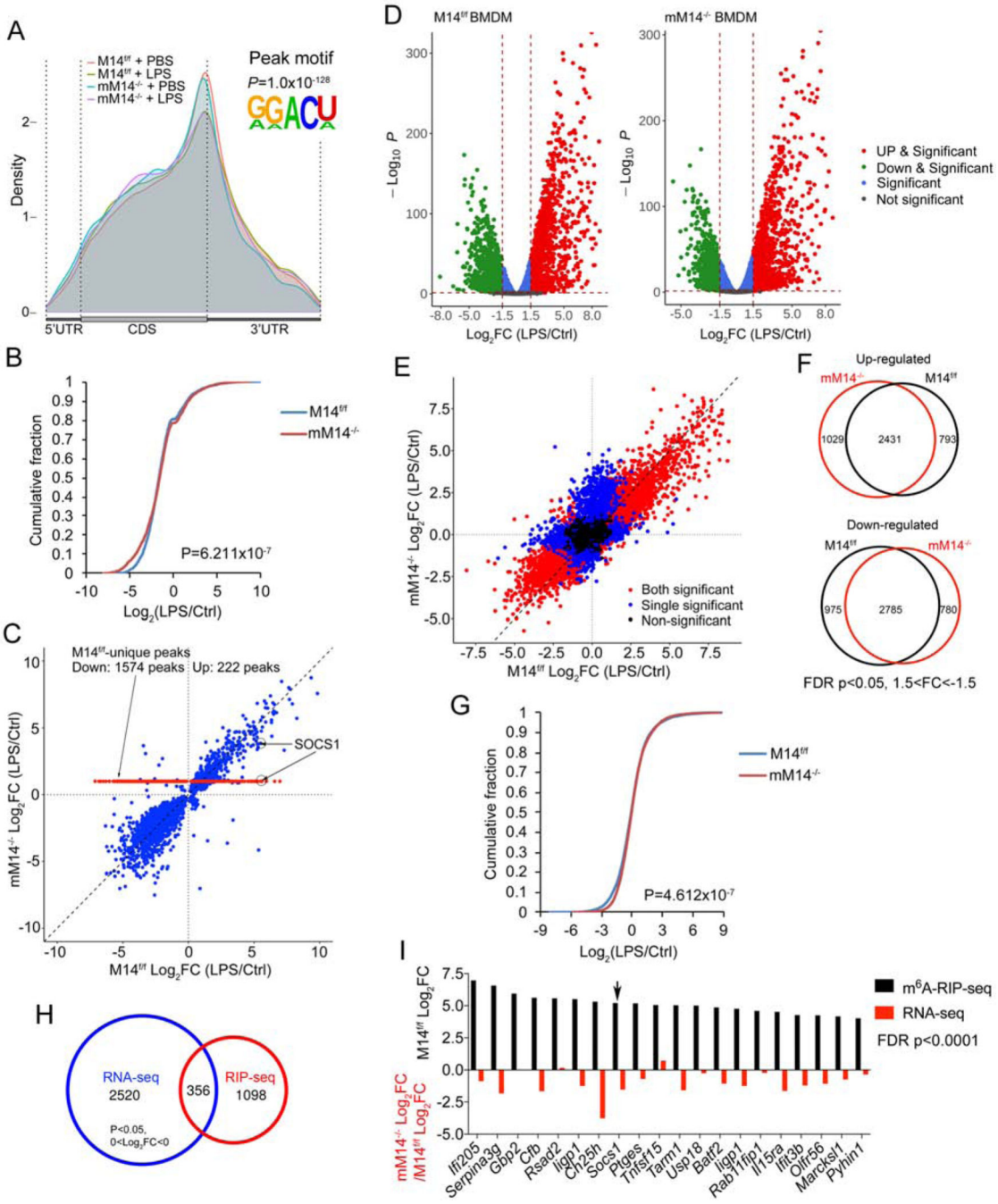

Figure 2. SOCS1 is a key METTL14 target in the regulation of macrophage activation.

(A) The m^{6}A peak distribution and m^{6}A motif identified by RIP-seq in M14$^{f/f}$ and mM14$^{-/-}$ BMDMs treated with PBS (Ctrl) or LPS;

(B) Cumulative fractions of LPS-induced or -reduced m^{6}A peaks in M14$^{f/f}$ and mM14$^{-/-}$ BMDMs;

(C) Correlation plots of LPS-induced or -reduced m^{6}A peaks in M14$^{f/f}$ and mM14$^{-/-}$ BMDMs. M14$^{f/f}$-unique LPS-induced m^{6}A peaks and LPS-induced *Socs1* m^{6}A peaks are indicated by *arrows*. Note many transcripts have multiple m^{6}A peaks.

(D) RNA-seq volcano plots of $M14^{f/f}$ and $mM14^{-/-}$ BMDMs treated with PBS (Ctrl) or LPS;
(E) Correlation plots of LPS-induced or -reduced transcripts between $M14^{f/f}$ and $mM14^{-/-}$ BMDMs;
(F) Number and relationship of transcripts up-regulated or down-regulated by LPS between $M14^{f/f}$ and $mM14^{-/-}$ BMDMs;
(G) Cumulative fractions of LPS-induced or -reduced transcripts in $M14^{f/f}$ and $mM14^{-/-}$ BMDMs;
(H) Relationship between the $M14^{f/f}$-unique m^6A peaks and mRNA transcripts whose LPS-induced log_2FC between $mM14^{-/-}$ and $M14^{f/f}$ cells is >0 or <0;
(I) Top 20 $M14^{f/f}$-unique m^6A peaks according to LPS-induced Log_2FC and their corresponding transcript's LPS-induced log_2FC ratio between $mM14^{-/-}$ and $M14^{f/f}$ cells. *Socs1* is indicated by an *arrow*.

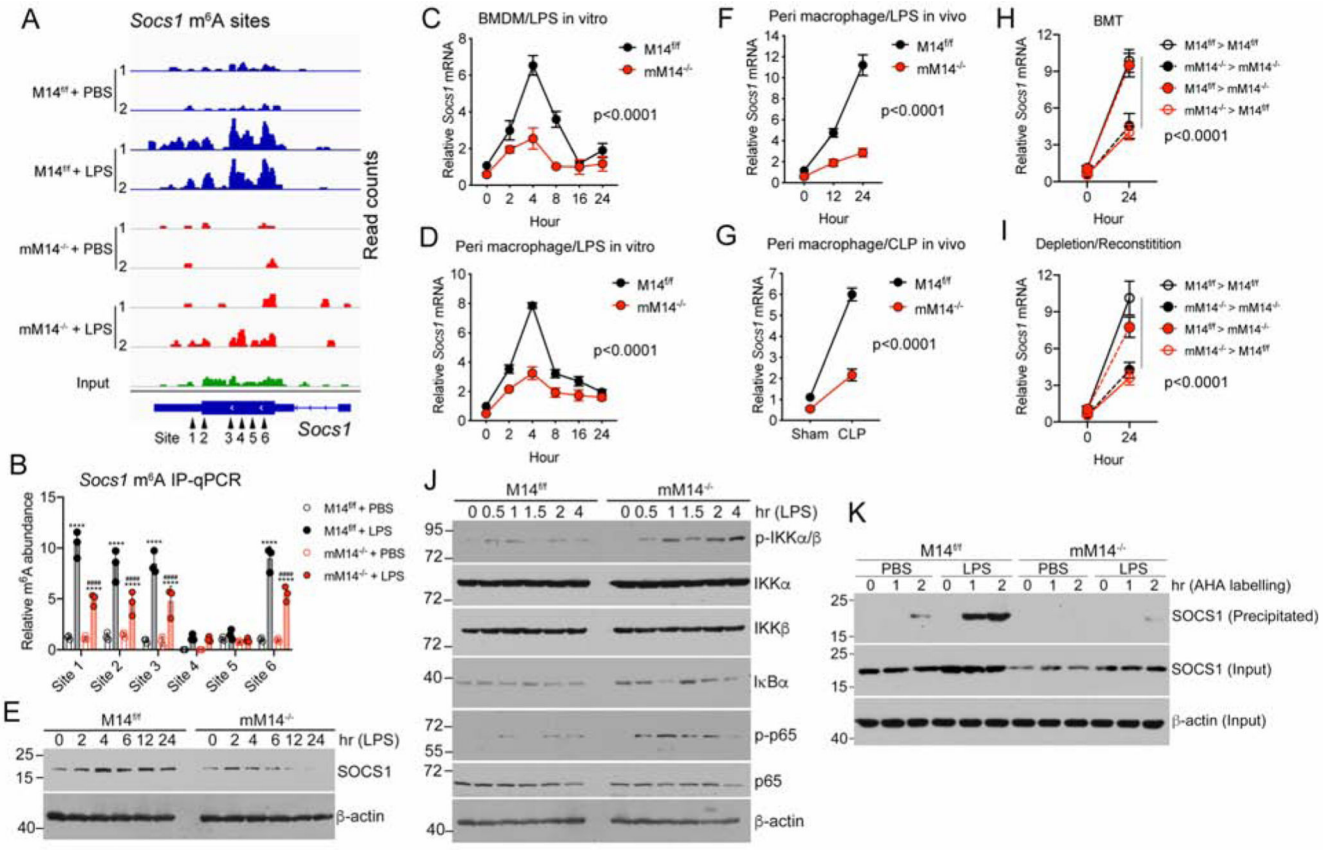

Figure 3. METTL14 is required for *Socs1* mRNA m^{6}A methylation and SOCS1 induction in macrophage activation.

(A) Read density in *Socs1* transcript in M14$^{f/f}$ and mM14$^{-/-}$ BMDMs treated with PBS (Ctrl) or LPS. Six sites (Sites 1–6) on the *Socs1* transcript that are associated with LPS-induced m^{6}A peaks are indicated;

(B) RIP-qPCR assays validating the LPS-induced m^{6}A peaks on *Socs1* transcript in M14$^{f/f}$ BMDMs and reduced peak inductions in mM14$^{-/-}$ BMDMs. The cells were treated with PBS or LPS for 6 hrs; ****p < 0.0001 verse corresponding PBS; ####p < 0.0001 verse corresponding LPS, by two-way ANOVA.

(C, D) Time course of *Socs1* mRNA expression in cultured M14$^{f/f}$ and mM14$^{-/-}$ BMDMs (C), or peritoneal macrophages (D) treated with LPS; n=3 at each time point in each group;

(E) Time course of SOCS1 protein expression in M14$^{f/f}$ and mM14$^{-/-}$ BMDMs treated with LPS;

(F,G) *Socs1* mRNA expression in peritoneal macrophages freshly isolated from mice treated with LPS for 0, 12 and 24 hrs (F) or following CLP surgery for 24 hrs (G);

(H,I) *Socs1* mRNA expression in peritoneal macrophages freshly isolated from BMT recipient mice (See Figure S3) challenged with LPS for 24 hrs (H), or from macrophage-depleted mice reconstituted with BMDMs (See Figure S4) and treated with LPS for 24 hrs (I);

(J) NF-κB signaling over time in M14$^{f/f}$ and mM14$^{-/-}$ BMDMs following LPS stimulation;

(K) L-azidohomoalanine (AHA) pulse labelling of newly translated SOCS1 protein in PBS- or LPS-reated M14$^{f/f}$ and mM14$^{-/-}$ BMDMs. The cells were pulse-labelled with AHA for 0,

1 and 2 hrs before the labelled proteins were precipitated with streptavidin beads. Precipitated AHA-labelled SOCS1 protein and total SOCS1 in the input were visualized by anti-SOCS1 antibody.

Data are presented as mean ± SD.

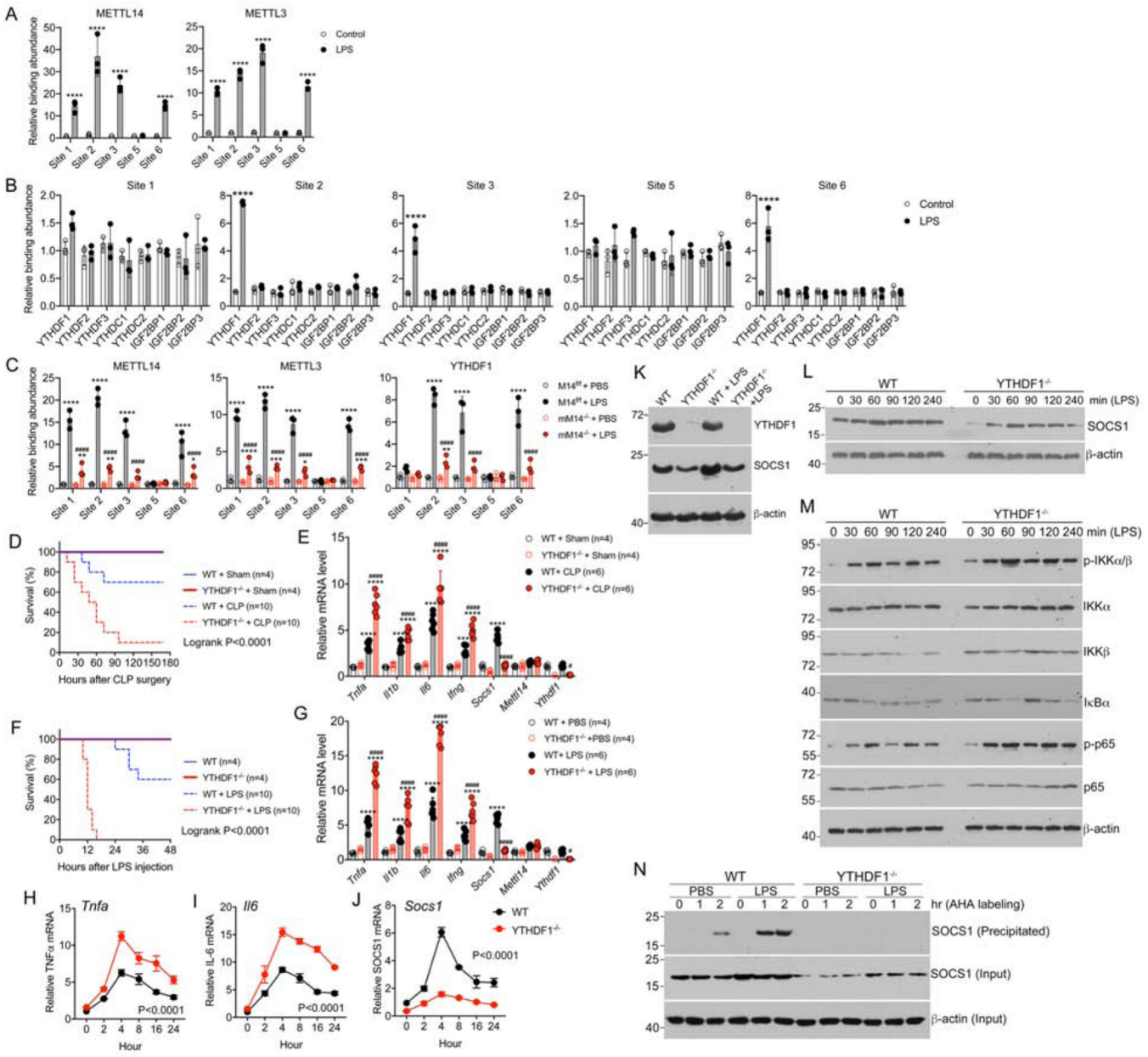

Figure 4. YTHDF1 is the reader to mediate the activities of *Socs1* m^{6}A in macrophage activation.

(A) CLIP assays showing the binding of METTL14 and METTL3 to the *Socs1* m^{6}A sites in RAW264.7 cells treated with PBS (Control) or LPS for 6 hrs; ****p < 0.0001 verse corresponding Control, by two-way ANOVA.

(B) CLIP assays assessing the binding of readers to the *Socs1* m^{6}A sites in RAW264.7 cells treated with PBS (Control) or LPS for 6 hrs; ****p < 0.0001 verse the rest, by two-way ANOVA. Data are presented as mean ± SD.

(C) CLIP assays assessing the interactions of METTL14, METTL3 and YTHDF1 with the *Socs1* m^{6}A sites in M14$^{f/f}$ and mM14$^{-/-}$ BMDMs treated with PBS or LPS for 6 hrs;

(D) Kaplan-Meier survival curves of WT and YTHDF1$^{-/-}$ mice after CLP or sham surgery;

(E) Expression of cytokine and *Socs1* transcripts in freshly isolated peritoneal macrophages from WT and YTHDF1$^{-/-}$ mice 24 hrs after CLP surgery;
(F) Survival curves of WT and YTHDF1$^{-/-}$ mice following LPS challenge;
(G) Expression of cytokine and *Socs1* transcripts in freshly isolated peritoneal macrophages from WT and YTHDF1$^{-/-}$ mice 24 hrs after LPS challenge;
(H-J) Time course expression of TNF- α (H), IL-6 (I) and Socs1 (J) transcripts in WT and YTHDF1$^{-/-}$ BMDMs following LPS treatment;
*P<0.05; **P<0.01; ***P<0.001, ****P<0.0001 vs. corresponding Sham or PBS; $^{\#\#\#}$P<0.001, $^{\#\#\#\#}$P<0.0001 vs. corresponding CLP or LPS, by two-way ANOVA. Data are presented as mean ± SD.
(K) YTHDF1 and SOCS1 expression in WT and YTHDF1$^{-/-}$ BMDMs with or without LPS treatment;
(L) Time course induction of SOCS1 protein in LPS-treated WT and YTHDF1$^{-/-}$ BMDMs;
(M) NF-κB signaling over time in WT and YTHDF1$^{-/-}$ BMDMs following LPS stimulation;
(N) AHA pulse labelling of newly translated SOCS1 protein in PBS- or LPS-treated WT and YTHDF1$^{-/-}$ BMDMs. The cells were pulse-labelled with AHA for 0, 1 and 2 hrs before the labelled proteins were precipitated with streptavidin beads. Precipitated AHA-labelled SOCS1 protein and total SOCS1 in the input were visualized by anti-SOCS1 antibody.

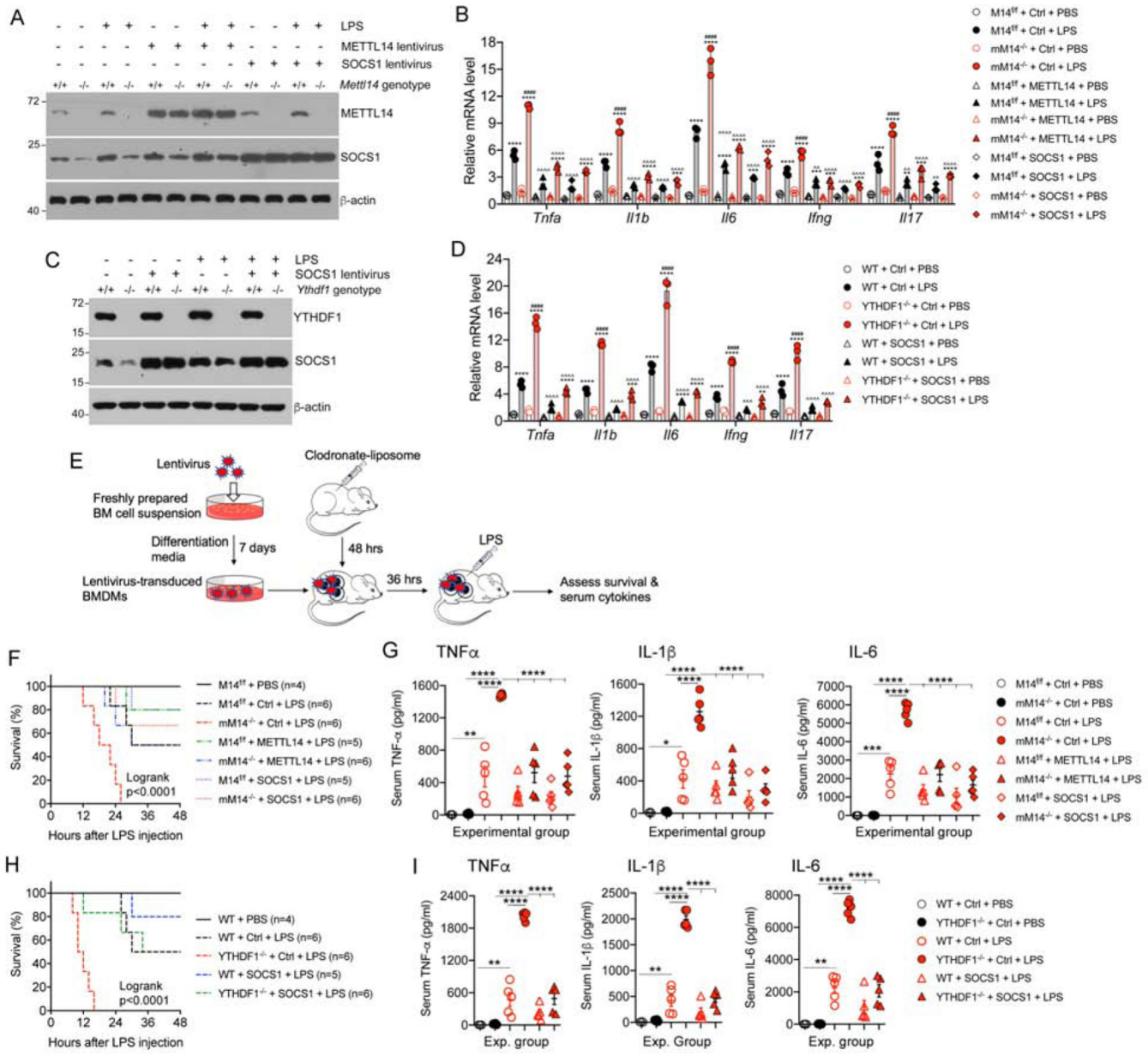

Figure 5. Forced expression of SOCS1 corrects the hyper inflammatory abnormalities of mM14$^{-/-}$ and YTHDF1$^{-/-}$ macrophages in cultures and in mice.

(A) M14$^{f/f}$ and mM14$^{-/-}$ BMDMs were transduced with METTL14-lentivirus, SOCS1-lentivirus or control virus (−), and then treated with LPS or PBS (−). METTL14 and SOCS1 expression was assessed by Western blotting;

RT-qPCR quantitation of pro-inflammatory cytokines in M14$^{f/f}$ and mM14$^{-/-}$ BMDMs infected with control (Ctrl) lentivirus, METTL14-lentivirus or SOCS1-lentivirus and treated with PBS or LPS for 6 hrs; **p < 0.01; ***p < 0.001, ****p < 0.0001 verse corresponding PBS; ####p < 0.0001 verse corresponding M14$^{f/f}$ + Ctrl + LPS; ^^p < 0.01, ^^^p < 0.001, ^^^^p < 0.0001 verse corresponding M14$^{f/f}$ + Ctrl + LPS or mM14$^{-/-}$ + Ctrl + LPS, respectively; by two-way ANOVA.

(C) WT and YTHDF1$^{-/-}$ BMDMs were transduced with SOCS1-lentivirus or control virus (−) and then treated with LPS or PBS (−). YTHDF1 and SOCS1 expression was assessed by Western blotting;

(D) RT-qPCR quantitation of pro-inflammatory cytokines in WT and YTHDF1$^{-/-}$ BMDMs infected with Ctrl lentivirus or SOCS1-lentivirus and treated with PBS or LPS for 6 hours; **p < 0.01; ***p < 0.001, ****p < 0.0001 verse corresponding PBS; ####p < 0.0001 verse corresponding WT + Ctrl + LPS; ^^^ p < 0.001, ^^^^p < 0.0001 verse corresponding WT + Ctrl + LPS or YTHDF1$^{-/-}$ + Ctrl + LPS, respectively; by two-way ANOVA.

(E) Illustration of macrophage depletion and reconstitution procedure;

(F) Survival curves of macrophage-depleted mice reconstituted with M14$^{f/f}$ or mM14$^{-/-}$ BMDMs transduced with METTL14-lentivirus, SOCS1-lentivirus or Ctrl virus after LPS challenge; P<0.0001 mM14$^{-/-}$ + Ctrl + LPS vs. the rest.

(G) Serum cytokine concentrations in macrophage-depleted mice reconstituted with M14$^{f/f}$ or mM14$^{-/-}$ BMDMs transduced with METTL14-lentivirus, SOCS1-lentivirus or Ctrl virus after LPS challenge.

(H) Survival curves of macrophage-depleted mice reconstituted with WT or YTHDF1$^{-/-}$ BMDMs transduced with SOCS1-lentivirus or Ctrl lentivirus after LPS challenge; P<0.0001 YTHDF1$^{-/-}$ + Ctrl + LPS vs. the rest.

(I) Serum cytokine concentrations in macrophage-depleted mice reconstituted with WT or YTHDF1$^{-/-}$ BMDMs transduced with SOCS1-lentivirus or Ctrl lentivirus after LPS challenge. *P<0.05, **P<0.01; ***P<0.001, ****P<0.0001, by one-way ANOVA. All data are presented as mean ± SD.

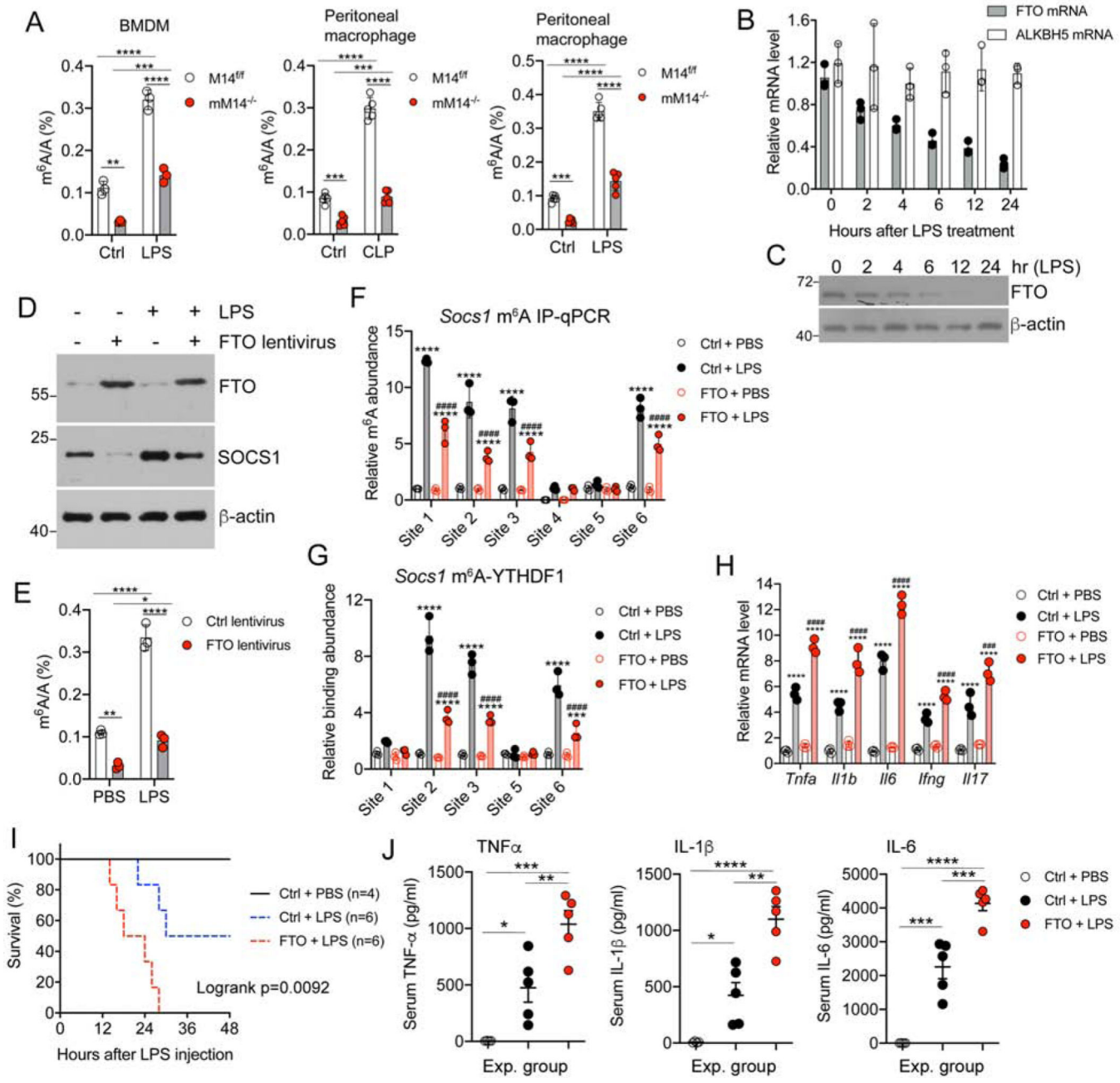

Figure 6. FTO regulates *Socs1* m^{6}A methylation in macrophage activation.

(A) Quantitation of m^{6}A in cultured M14$^{f/f}$ and mM14$^{-/-}$ BMDMs or in peritoneal macrophages freshly isolated from CLP-treated or LPS-treated M14$^{f/f}$ and mM14$^{-/-}$ mice; **P<0.01; ***P<0.001, ****P<0.0001; by two-way ANOVA.

(B) Time course RT-qPCR quantitation of *Alkbh5* and *Fto* transcripts in RAW264.7 cells treated with LPS;

(C) Time course expression of FTO protein in RAW264.7 cells treated with LPS;

(D) FTO and SOCS1 protein expression in RAW264.7 cells infected with control lentivirus (−) or FTO-lentivirus (+) and then treated with PBS (−) or LPS (+) for 6 hrs;

(E) Quantitation of total m^6A in Ctrl lentivirus or FTO-lentivirus infected RAW264.7 cells treated with PBS or LPS for 6 hrs; *P<0.05, **P<0.01; ***P<0.001, ****P<0.0001 by two-way ANOVA;

(F) Quantitation of *Socs1* m^6A by m^6A-IP-qPCR in Ctrl lentivirus or FTO-lentivirus infected RAW264.7 cells treated with PBS or LPS;

(G) Quantitation of *Scos1* m^6A-YTHDF1 interactions by CLIP-qPCR in Ctrl lentivirus or FTO-lentivirus infected RAW264.7 cells treated with PBS or LPS;

(H) RT-qPCR quantitation of cytokine transcripts in Ctrl lentivirus or FTO-lentivirus infected BMDMs treated with PBS or LPS for 6 hrs. ****P<0.0001 vs. corresponding PBS; ####P<0.0001 vs. corresponding Ctrl + LPS; by two-way ANOVA; Data are mean ± SD.

(I) Survival curves of macrophage-depleted mice reconstituted with Ctrl lentivirus or FTO-lentivirus transduced BMDMs after LPS challenge;

(J) Serum cytokine concentrations in macrophage-depleted mice reconstituted with Ctrl lentivirus or FTO-lentivirus transduced BMDMs after LPS challenge; *P<0.05, **P<0.01; ***P<0.001, ****P<0.0001 by two-way ANOVA.

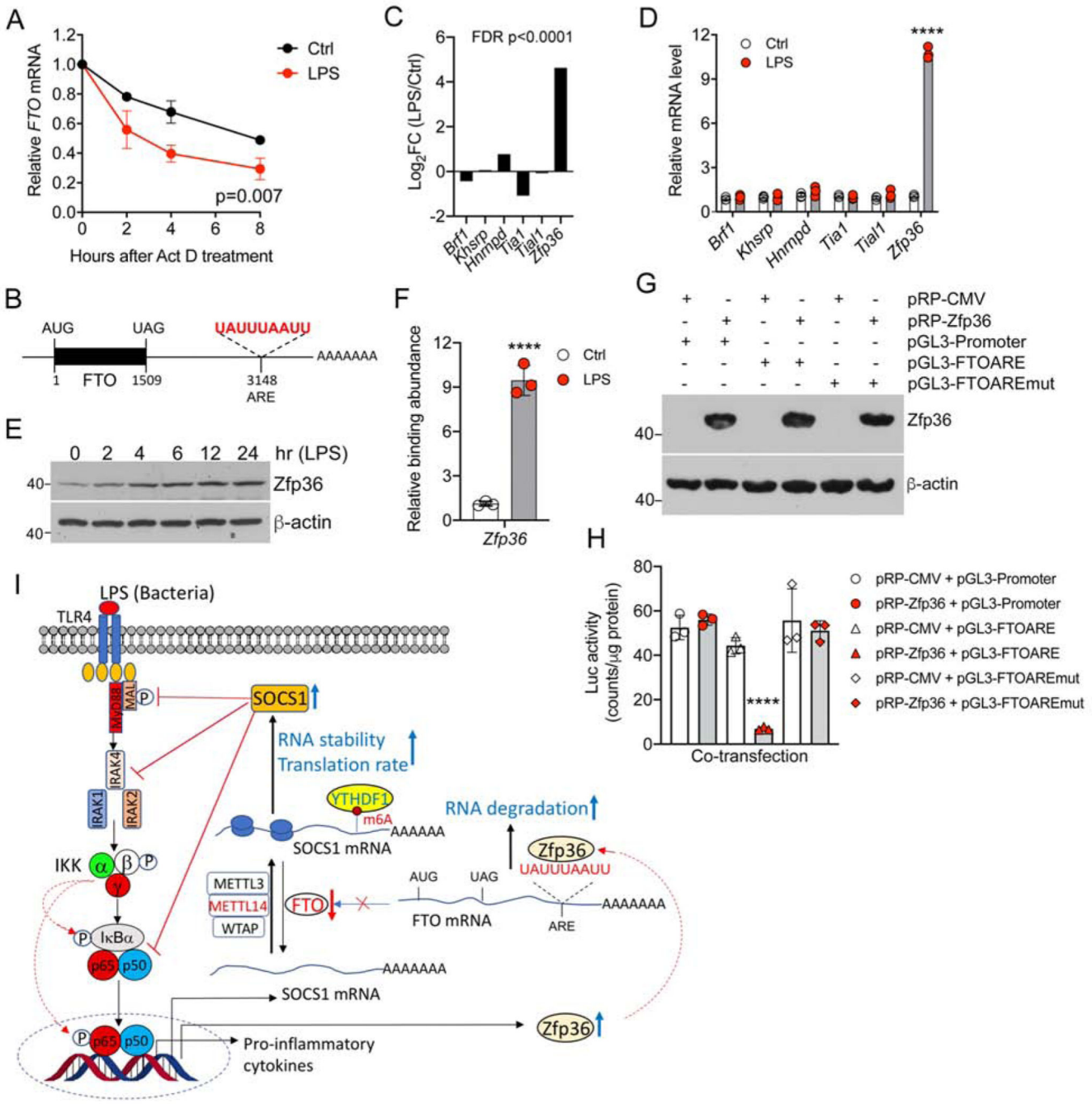

Figure 7. Zfp36 promotes *Fto* mRNA degradation in macrophage activation and the schematic conclusion.

(A) Fto mRNA decays in BMDMs treated with PBS (Ctrl) or LPS;

(B) Illustration of a highly conserved AU-rich element (ARE) in 3'UTR of mouse *Fto* transcript;

(C) LPS-induced Log_2FC of six known ARE-binding protein transcripts in RNA-seq data;

(D) RT-qPCR quantitation of six known ARE-binding proteins in RAW264.7 cells treated with PBS (Ctrl) or LPS; **** P<0.0001 vs. the rest.

(E) Time course of Zfp36 protein expression in RAW264.7 cells treated with LPS;

(F) CLIP-qPCR quantitation of Zfp36 binding to the FTO ARE site in RAW264.7 cells treated with PBS (Ctrl) or LPS; ****P<0.001 vs. Ctrl.
(G) Demonstration of Zfp36 expression in HEK293 cells co-transfected with a luciferase reporter plasmid and Zfp36-expressing plasmid;
(H) Luciferase activities from assays in various co-transfections as indicated; **** P<0.001 vs. the rest. Statistical analyses are by two-way ANOVA.
(I) Schematic summary of a mechanism whereby METTL14, YTHDF1 and FTO regulate *Socs1* m^6A methylation to sustain an appropriate SOCS1 level so that the negative feedback loop in LPS/TLR4 signaling is maintained to control macrophage inflammatory response.

KEY RESOURCES TABLE

Reagent or Resource	Source	Identifier
Antibodies		
Anti-β-actin	Santa Cruz Biotechnology	Cat#: sc-47778, RRID: AB_2714189
Anti-mouse IgG-HRP	Santa Cruz Biotechnology	Cat#: sc-516102, RRID: AB_2687626
Anti-rabbit IgG-HRP	Santa Cruz Biotechnology	Cat#: sc-2357, RRID: AB_628497
Anti-YTHDF3	Santa Cruz Biotechnology	Cat#: sc-377119, RRID: AB_2687436
Anti-YTHDC2	Santa Cruz Biotechnology	Cat#: sc-249370; RRID: N/A
Anti-YTHDF1	ProteinTech	Cat#: 17479-1-AP, RRID: AB_2217473
Anti-YTHDF2	ProteinTech	Cat#: 24744-1-AP, RRID: AB_2687435
Anti-ZFP36	ProteinTech	Cat#: 12737-1-AP, RRID: AB_10598485
Anti-YTHDC1	ProteinTech	Cat#: 14392-1-AP, RRID: N/A
Anti-IGF2BP3	ProteinTech	Cat#: 14642-1-AP, RRID: AB_2122782
Anti-IKKα	Cell Signaling Technology	Cat#: 11930, RRID: AB_2687618
Anti-IKKβ	Cell Signaling Technology	Cat#: 8943, RRID: AB_11024092
Anti-Phospho-IKKα/β	Cell Signaling Technology	Cat#: 2697, RRID: AB_2079382
Anti-Phospho-NF-κB p65	Cell Signaling Technology	Cat#: 3033, RRID: AB_331284
Anti-IκBα	Cell Signaling Technology	Cat#: 4814, RRID: AB_390781
Anti-NF-κB p65	Cell Signaling Technology	Cat#: 8242, RRID: AB_10859369
Anti-IGF2BP1	Cell Signaling Technology	Cat#: 8482S, RRID: AB_11179079
Anti-IGF2BP2	Cell Signaling Technology	Cat#: 14672S, RRID: AB_2798563
Anti-FTO	Abcam	Cat#: ab92821, RRID: AB_10565042
Anti-TLR4	Abcam	Cat#: ab13556, RRID: AB_300457
Anti-SOCS1	ThermoFisher Scientific	Cat#: 38–5200, RRID: AB_2533372
Anti-m6A	Synaptic Systems	Cat#: 202003, RRID: AB_2279214
Anti-METTL14	Sigma-Aldrich	Cat#: HPA038002, RRID: AB_10672401
Anti-METTL3	Aviva Systems Biology	Cat#: ARP39390_T100, RRID: AB_2142045
Anti-mouse MHCII FITC	BioLegend	Cat#: 107605, RRID: AB_313320
Anti-mouse CD11b perCP	BioLegend	Cat#: 101229, RRID: AB_2129375
Anti-mouse CD11c PE	BioLegend	Cat#: 117307, RRID: AB_313776
Anti-mouse F4/80 APC	BioLegend	Cat#: 123115, RRID: AB_893493
Chemicals, Peptides and Recombinant Proteins		
LPS from *E coli* O111:B4	Sigma-Aldrich	Cat#: L2630
Actinomycin D	Sigma-Aldrich	Cat#: A9415
Poly (I:C)	Sigma-Aldrich	Cat#: P1530
L-Azidohomoalanine	Click Chemistry Tools	Cat#: 1066–25
Biotin-PEG4-Alkyne	Click Chemistry Tools	Cat#: TA105-5
Critical Commercial Assays		
Luciferase Reporter Assay System	Promega	Cat#: G7941

Reagent or Resource	Source	Identifier
QuikChange XL Site-Directed Mutagenesis Kit	Agilent Technologies	Cat#: 200517
LIVE/DEAD™ Viability/Cytotoxicity Kit	Invitrogen	Cat#: L3224
SYBR Green Realtime PCR Master Mix kit	TOYOBO	Cat#: QPK-201
ReverTra Ace qPCR RT Kit	TOYOBO	Cat#: FSQ-101
Dynabeads mRNA Purification kit	Thermo Fisher	Cat#: 61006
RPMI1640, no methionine	Thermo Fisher	Cat#: A1451701
RNA Fragmentation Reagents	Thermo Fisher	Cat#: AM8740
SMARTer Stranded RNA-Seq Kit	TaKaRa	Cat#: 634836
SMARTer Stranded RNA-Seq Kit v2-Pico Input Mammalian	TaKaRa	Cat#: 634411
N6-Methyladenosine Enrichment Kit	New England Biolabs	Cat#: E1610S
Magnetic protein G beads	New England Biolabs	Cat#: S1430S
EpiQuik m6A RNA Methylation Quantification Kit	EPIGENTEK	Cat#: P-9005-48
Standard Macrophage Depletion Kit	Encapsula Nano Sciences	Cat#: CLD-8901
Mouse IL-1β ELISA Kit	BioLegend	Cat#: 432604
Mouse IFN-γ ELISA Kit	BioLegend	Cat#: 430804
Mouse IL-6 ELISA Kit	BioLegend	Cat#: 431304
Mouse TNF-α ELISA Kit	BioLegend	Cat#: 430904
Protein Reaction Buffer kit	Click Chemistry Tools	Cat#: 1262
Streptavidin Magnetic Beads	Click Chemistry Tools	Cat#:1497–1
Deposited Data		
RNA-seq (Raw and analyzed data)	This study	GEO: GSE153512
m6A-seq (Raw and analyzed data)	This study	GEO: GSE153511
Experimental Models: Cell Lines		
HEK293T	ATCC	Cat#: CRL-3216
RAW264.7	ATCC	Cat#: TIB-71
L929	ATCC	Cat#: CCL-1
Experimental Models: Organisms/Strains		
Mettl14(flox/flox) mice	Chuan He	N/A
YTHDF1(−/−) mice	Chuan He	N/A
B6.129P2-Lyz2tm1(cre)Ifo/J	Jackson Laboratory	Stock No: 004781
Oligonucleotides		
All oligonucleotide sequences are listed in Supplemental Table S1.		
Recombinant DNA		
pGL3-Promoter	Promega	Cat#: E1761
pGL3-FTOARE	This study	N/A
pGL3-FTOAREmutant	This study	N/A
pRP-CMV	VectorBuilder	N/A
pRP-mZfp36	VectorBuilder	ID: VB200224-1085evp

Reagent or Resource	Source	Identifier
pLV-Neo-EF1A-hMETTL14	VectorBuilder	ID: VB191018-1246kgq
pLV-Neo-EF1A-hFTO-	VectorBuilder	ID: VB191018-1248dvj
pLV-Neo-EF1AhSOCS1	VectorBuilder	ID: VB191018-1238kwr
pLV-Neo-EF1A-GFP	VectorBuilder	N/A
Software and Algorithms		
ImageJ	NIH	https://imagej.nih.gov/ij/
FlowJo software V10	BD	https://www.flowjo.com/
trim_galore v0.6.5	Babraham Institute	https://www.bioinformatics.babraham.ac.uk/projects/trim_galore/
STAR v2.6.1d	(Dobin et al., 2013)	https://code.google.com/archive/p/rna-star/
Hisat2 software	(Kim et al., 2015)	http://www.ccb.jhu.edu/software/hisat/index.shtml
exomePeak-2.8.0	(Meng et al., 2013)	http://compgenomics.utsa.edu/exomePeak/
HOMER v4.10.0	(Heinz et al., 2010)	http://homer.ucsd.edu/homer/changeLog.html
Prism 8.4.2	GraphPad	https://graphpad-prism.software.informer.com